OENO One
vine & wine

DOI: https://doi.org/10.20870/oeno-one.2026.60.3.9877

OPEN ACCESS



SPECIAL ISSUE

On-the-go hyperspectral imaging for monitoring grape maturity in Tempranillo: supporting adaptive harvest decisions

Aitana Tejada-González[1,2], Ignacio Barrio[1,2], Leonardo Poggi[3], Juan Fernández-Novales[1,2], Leticia Martínez-Lapuente[1,2], Zenaida Guadalupe[1,2], María P. Diago[1,2,*]

[1] University of La Rioja, Department of Agricultural and Food Science. Madre de Dios 53, 26006. Logroño. La Rioja (Spain)
[2] Institute of Grapevine and Wine Sciences. Finca La Grajera. Ctra. de Burgos Km. 6. 26007. Logroño. La Rioja (Spain)
[3] University of Bologna, Department of Agricultural and Food Science. G. Fanin 44, 40127. Bologna, (Italy)

Article number: 9877

*correspondence:
maria-paz.diago@unirioja.es

Associate editor:
Cécile Coulon-Leroy

Received:
29 January 2026

Accepted:
05 May 2026

Published:
01 July 2026

This article is published under the **Creative Commons licence** (CC BY 4.0).

Use of all or part of the content of this article must mention the authors, the year of publication, the title, the name of the journal, the volume, the pages and the DOI in compliance with the information given above.

KEYWORDS: proximal sensing, berry composition, chemometrics, *Vitis vinifera*, precision viticulture, TERCLIM 2026

This article is an original research article published in cooperation with the 16th International Terroir Congress and the 3rd ClimWine Symposium (July 5–9, 2026), hosted by the École Supérieure des Agricultures in Angers, France.

Guest editors: Cécile Coulon-Leroy and Etienne Neethling.

ABSTRACT

Climate change is disrupting grapevine phenology and threatening terroir-driven wine typicity, challenging the definition of optimal harvest timing. This study develops and validates an on-the-go dual-range hyperspectral imaging workflow for non-destructive, real-time monitoring of grape maturity in *Vitis vinifera* L. cv. Tempranillo. The system integrates two pushbroom cameras – visible to near-infrared (400–1000 nm) and short-wave infrared (900–1700 nm) – mounted on a mobile platform operating under field conditions. Over seven sampling dates from veraison to harvest (August – September 2025), hyperspectral images were collected in a commercial vineyard in Logroño (La Rioja, Spain). Corresponding reference analyses included total soluble solids, pH, titratable acidity, tartaric acid, malic acid, yeast-assimilable nitrogen, anthocyanins, total phenolic index, colour intensity, and chromatic coordinates L^*, a^* and b^*.

Partial least squares regression models were developed to predict grape composition parameters from processed hyperspectral data. Model performance was assessed through independent prediction, exhibiting very good to excellent predictive performance for key technological maturity traits: titratable acidity (R^2_p = 0.98), malic acid (R^2_p = 0.95), total soluble solids (R^2_p = 0.94), and pH (R^2_p = 0.93). Chromatic attributes also showed reliable estimations, particularly colour intensity (R^2_p = 0.88), b^* (R^2_p = 0.89), and a^* (R^2_p = 0.88), with L^* reaching an R^2_p of 0.81. Tartaric acid (R^2_p = 0.79) and total phenolic index (R^2_p = 0.76) achieved good quantitative accuracy, while anthocyanins (R^2_p = 0.58) and yeast-assimilable nitrogen (R^2_p = 0.56) provided satisfactory discrimination for vineyard screening purposes.

The high performance for malic acid highlights the relevance of including the short-wave infrared spectral range, where absorption features of organic acids are more pronounced. This work represents, to the best of our knowledge, the first field-based demonstration of yeast-assimilable nitrogen prediction from hyperspectral data, expanding the analytical scope of proximal sensing for viticulture.

The proposed on-the-go hyperspectral imaging framework offers a practical, scalable tool for adaptive harvest decision-making under increasing climate variability. It supports the maintenance of varietal typicity and wine style consistency by facilitating timely, data-driven harvest scheduling. Future work will extend model validation across seasons and sites and explore advanced modelling approaches to support operational deployment.

INTRODUCTION

Climate change is altering grapevine phenology and increasing interannual variability in ripening patterns, thus challenging traditional harvest scheduling and threatening the consistency of *terroir* expression. Notably, rising temperatures are causing the advancement and acceleration of key phenological stages – flowering, veraison, and ripeness – whilst shortening the interval between budbreak and harvest (Droulia & Charalampopoulos, 2021; van Leeuwen *et al.*, 2024). As a consequence, ripening increasingly occurs under warmer conditions, leading to faster and often excessive sugar accumulation, whereas the biosynthesis of anthocyanins and volatile compounds does not necessarily follow the same trajectory (Rienth *et al.,* 2021; Jones *et al*., 2022). This growing asynchrony between sugar-acid dynamics and the development of phenolic and aromatic attributes has been widely documented and represents one of the major challenges for contemporary viticulture under climate change (van Leeuwen & Destrac-Irvine, 2017; Cosme *et al.,* 2024).

These shifts pose critical threats for premium wine regions, where typicity and stylistic consistency depend on the delicate balance between technological, phenolic, and aromatic maturity. In Rioja Qualified Designation of Origin (northern Spain), *Vitis vinifera* L. cv. Tempranillo – the emblematic red variety representing over 80 % of the appellation's vineyard area and the third most cultivated grape variety for red wine production globally (Anderson *et al*., 2024) – is particularly vulnerable to climate-driven compositional imbalances. This cultivar, which arose from the spontaneous cross between 'Albillo Mayor' and 'Benedicto' (Ibáñez *et al*., 2012), is recognised as the noblest Spanish variety and sustains the international prestige of Rioja wines. However, 'Tempranillo' is an earlyripening cultivar with a relatively short vegetative cycle (Cervera *et al.*, 2002), features that compromise its adaptation to projected climate scenarios. In comparative studies across Rioja DOCa, Ramos and de Toda (2021) demonstrated that 'Graciano' exhibits better resilience than 'Tempranillo' under warming conditions, maintaining more favourable acidity levels and phenolic balance. The early phenology and naturally low acidity of 'Tempranillo' render it particularly susceptible to the compositional imbalances exacerbated by rising temperatures and heat waves, which decouple sugar accumulation from organic acid retention and phenolic development, threatening the region's signature style (Ramos & de Toda, 2020, Ramos & de Toda, 2021).

Defining optimal harvest timing thus requires integrating multiple, often conflicting, changes in grape composition during ripening – sugars, acidity (particularly malic acid dynamics), phenolic compounds, and nitrogen status – that evolve at different rates and respond differently to environmental stress. In practice, the optimal harvest window can be narrow, often in the order of only a few days, particularly in warm vintages (van Leeuwen *et al*., 2019). Harvesting too early may result in insufficient sugar accumulation, elevated acidity, and underdeveloped phenolic and aromatic profiles, leading to wines lacking colour intensity, structure, and sensory complexity (Sadras & Moran, 2012; Plantevin *et al*., 2024). Conversely, delaying harvest to achieve adequate phenolic or aromatic maturity can promote excessive sugar concentrations, low acidity, and the emergence of overripe or cooked fruit sensory notes, which compromise freshness, balance, and typicity (Allamy *et al*., 2023). These findings highlight that suboptimal harvest decisions not only affect technological parameters but also have profound consequences for the sensory identity and ageing potential of wines, reinforcing the need for integrated, multi-parameter approaches to ripeness assessment under climate change.

Yet conventional vineyard sampling remains a major bottleneck for precision harvest management. Traditional maturity assessment relies largely on destructive sampling and laboratory analyses of a limited number of berries (for example, 200 berries per block) mainly focused on total soluble solids and titratable acidity. These conventional approaches are labour-intensive, time-consuming, and provide delayed feedback, while offering limited spatial resolution (Ye *et al*., 2023).

Spatial heterogeneity in grape composition, driven by variations in soil, topography, water status, and canopy microclimate, has been widely documented (Baluja *et al*., 2013; Minnaar *et al*., 2022; Sams *et al.,* 2022; Verdugo-Vásquez *et al.,* 2022). Despite this variability, harvesting is frequently conducted uniformly, mixing grapes of different maturity levels and potentially diluting wine quality and economic value (Bramley *et al*., 2003). From a *terroir* perspective, this practice masks the fine-scale expression of site-specific characteristics, which are increasingly recognised as dynamic and spatially structured rather than homogeneous. Precision viticulture approaches have thus been proposed as a means of characterising and managing terroir variability at multiple scales, allowing the "sense of place" to be analysed, preserved, and leveraged rather than averaged out (Bramley *et al*., 2020; Tardáguila *et al*., 2021). For instance, González-Pavez *et al*. (2025) demonstrated the feasibility of spectral index-based contour mapping for non-destructive ripeness monitoring in water-stressed 'Cabernet-Sauvignon' vineyards, revealing spatial patterns of maturity heterogeneity that would remain undetected by conventional point sampling.

In this context, there is a growing demand for high-throughput, non-destructive, and spatially explicit tools capable of monitoring grape ripening dynamics in near real time. Hyperspectral imaging (HSI) technology addresses this need by integrating conventional imaging and spectroscopy to acquire spatially resolved spectral information across hundreds of contiguous narrow wavelengths (Goetz *et al.*, 1985). Unlike RGB or multispectral systems, HSI generates a three-dimensional data structure (a hypercube) that combines spatial (x, y) and spectral (λ) information, capturing a complete reflectance spectrum for each pixel in the image. This technique exploits electromagnetic radiation-matter interactions: spectral patterns comprising absorption,

scattering, and reflectance features arise from electronic transitions and molecular vibrations of key functional groups (C–H, O–H, N–H bonds), providing indirect information on pigments, water, sugars, proteins, acids, and other chemical constituents across the visible (VIS, 400–700 nm), near-infrared (NIR, 700–1000 nm), and short-wave infrared (SWIR, 1000–2500 nm) regions (Gowen *et al*., 2007; Hall *et al*., 2002).

Originally developed for remote sensing applications, HSI has evolved into a versatile analytical platform with demonstrated capabilities for detecting contaminants, performing non-destructive quality inspection, monitoring physiological status, and assessing ripeness and composition in fresh and processed foods (Gowen *et al*., 2007; Dale *et al*., 2013). For instance, HSI has been successfully used to monitor nutrient status, such as potassium content in sugar beet and celery, achieving high predictive accuracy (R^2 = 0.85 and 0.79, respectively) and supporting precision fertilisation strategies across species and developmental stages (Siedliska *et al.,* 2026). In leafy vegetables, deep learning models combined with hyperspectral data have enabled reliable freshness classification in spinach and Chinese cabbage, highlighting the potential of this technology for postharvest quality monitoring (He *et al.,* 2024). Similarly, hyperspectral imaging has been applied to seed classification, where multidimensional convolutional neural networks achieved accuracies above 90 % for rice variety identification (Jin *et al.,* 2025). Disease detection has also benefited from this technology, as early identification of pear leaf anthracnose using multi-source feature fusion achieved accuracies exceeding 98 %, enabling early warning and prevention strategies (Zhang *et al.,* 2024). Beyond crop health, ground-based hyperspectral systems have been used for mango yield prediction in orchard environments, providing reliable estimates and supporting precision agriculture applications (R^2 up to 0.83; Gutiérrez *et al.,* 2019b). In postharvest quality evaluation, hyperspectral imaging has enabled non-destructive prediction of internal attributes, such as firmness and soluble solids content in apples (Çetin *et al.,* 2022), sugar content in pears (Zhang *et al.,* 2018), and soluble solids in citrus fruit (Kim *et al.,* 2024). Additionally, hyperspectral techniques have been employed to detect contaminants and quality deterioration, including aflatoxin B1 in almonds (Mishra *et al.,* 2022) and postharvest quality decline in mushrooms during cold storage (Nazir *et al.,* 2022).

In viticulture, its application includes compositional assessment, grape variety classification, disease detection, screening for pesticide residues and monitoring of stress responses (Ye *et al*., 2023). Under controlled laboratory conditions, HSI has demonstrated remarkable predictive capabilities for grape quality parameters. Studies have achieved accurate estimation of total soluble solids (TSS), titratable acidity (TA), pH, and anthocyanins (R^2 > 0.85), as well as total phenolic compounds and skin maturity indices (Baiano *et al.,* 2012; Nogales-Bueno *et al.*, 2014; Chen *et al.,* 2015; Gomes *et al.,* 2017). More remarkably, HSI has proven capable of quantifying trace-level constituents present at microgram concentrations per berry: Marín-San Román *et al.* (2024) successfully predicted 20 individual volatile compounds in 'Tempranillo' grapes throughout ripening, including terpenoids, norisoprenoids, benzenoids, fatty acids, and C6 compounds, with cross-validation coefficients of determination (R^2_{cv}) ≥ 0.5 for most analytes. These findings demonstrate that HSI can capture a comprehensive chemical fingerprint of grape berries, enabling multi-parameter characterisation of the complex technological, phenolic, and aromatic maturity dynamics described above. However, despite the analytical depth demonstrated under laboratory conditions, certain compositionally relevant parameters remain uncharacterised by hyperspectral imaging. Notably, yeast-assimilable nitrogen (YAN) – comprising free amino acids and ammonium ions essential for fermentation kinetics and aroma biosynthesis (Bell & Henschke, 2005) – has not been previously predicted from hyperspectral data, likely due to its low concentration relative to other constituents, chemical heterogeneity, and spectral overlap with other nitrogenous compounds. Addressing this limitation broadens the scope of hyperspectral phenotyping, enabling a more detailed characterisation of grape compositional traits pertinent to winemaking.

Furthermore, the analytical scope and predictive performance of hyperspectral grape characterisation are strongly influenced by the spectral range employed. Whilst most grape quality studies have relied exclusively on VIS-NIR imaging (Baiano *et al.,* 2012; Fernández-Novales *et al.,* 2021; Bertoglio *et al.*, 2024) or, less commonly, on NIR-SWIR configurations starting beyond 900 nm (Nogales-Bueno *et al.,* 2014; Chen *et al.,* 2015), recent applications in other agricultural commodities have successfully employed dual-range VIS-SWIR systems for comprehensive quality assessment in persimmons (Zhao *et al.,* 2026) and smoked paprika (Alonso *et al.,* 2026). The dual-range configuration adopted in the present study, which integrates VIS-NIR and SWIR sensors to cover a continuous spectral range of 400–1700 nm, enables the exploitation of complementary spectral information across both ranges. Whilst the VIS-NIR region effectively captures sugar-related absorption bands and phenolic pigments, the extension into the SWIR may enhance sensitivity for organic acid characterisation, as malic and tartaric acids (MH_2 and TH_2, respectively) exhibit sharper, better-resolved absorption features beyond 1000 nm driven by the overtones and combination bands of their carboxylic functional groups (Williams & Norris, 2001; Cozzolino *et al.,* 2006; Pasquini, 2018).

Nevertheless, a critical gap persists between laboratory-based studies and field-deployable systems. Most published research has been conducted under controlled illumination on detached berries or clusters positioned at fixed distances from the sensor – conditions that do not reflect the complexity of commercial vineyard environments. Recent efforts have begun transitioning towards proximal sensing platforms mounted on ground vehicles, enabling on-the-go monitoring of grape composition directly in the field (Benelli *et al*., 2021; Fernández-Novales *et al*., 2021;

Bertoglio *et al*., 2024). However, field-based hyperspectral monitoring remains underexplored due to substantial technical challenges. Outdoor deployment is fundamentally constrained by illumination variability: hyperspectral sensors are highly susceptible to changes in ambient light intensity and spectral quality caused by solar angle, cloud cover, and canopy shadows (Cornelissen *et al*., 2025). The hyperspectral acquisition system developed in this study mitigated this limitation through a hybrid illumination strategy that involved combining natural sunlight with supplementary halogen lamps and radiometric calibration performed immediately before each acquisition session. Additional obstacles include variable camera-to-target distances, platform vibrations from terrain irregularities, and difficulties maintaining constant forward speeds, all of which introduce noise and artefacts that compromise spectral consistency (Gutiérrez *et al*., 2019a; Benelli *et al*., 2021). Moreover, the high-dimensional nature of hyperspectral data demands substantial computational infrastructure for real-time processing, storage, and transmission, whilst SWIR systems remain considerably more expensive than VIS-NIR sensors, adding complexity to the implementation of comprehensive dual-range platforms (ElMasry & Sun, 2010; Gomes *et al*., 2017). These technical and logistical constraints have limited the development of operational field-based systems capable of tracking the multiple compositional trajectories that define grape maturity under uncertain environmental conditions.

The present study addressed these gaps by developing and validating a dual-range (VIS-NIR and SWIR) on-the-go hyperspectral imaging workflow for non-destructive monitoring of grape maturity dynamics in 'Tempranillo' under field conditions. The objective was to establish predictive models for key compositional parameters – spanning technological, phenolic, and nitrogen-related attributes – capable of supporting data-driven harvest decisions under the increasingly unpredictable ripening patterns induced by climate change.

MATERIALS AND METHODS

The experimental workflow, illustrated in Figure 1, involved the on-the-go acquisition of hyperspectral images from grape clusters from veraison to commercial harvest. After imaging, reference grape composition data were obtained using established laboratory methods to characterise technological maturity parameters (TSS, pH, TA, organic acids, YAN) and phenolic attributes (anthocyanins, total phenolic index (TPI), colour intensity (CI), and CIELab coordinates). Spectral data extracted from berry pixels were preprocessed and modelled against reference analytical values using Partial Least Squares (PLS) regression. Model performance was evaluated using calibration, cross-validation, and independent prediction statistics to assess the capability of on-the-go hyperspectral imaging for non-destructive monitoring of grape maturity.

1. Experimental layout

The study was conducted during the 2025 growing season in a commercial *Vitis vinifera* L. cv. Tempranillo vineyard located at Monte Cantabria, northwest of Logroño city, La Rioja, Spain (42°28'48" N, 2°26'05" W, 490 m above sea level). The vineyard was planted in 1997 with vines grafted onto 110 Richter rootstock and trained to a vertical shoot positioning (VSP) system. Winter pruning was performed according to local practice, leaving four to five spurs per vine with two buds per spur.

Vines were spaced at 3.0 m between rows and 1.2 m within the row, resulting in a planting density of 2,922 vines ha^{-1}. The vineyard was managed following standard commercial practices for the region.

Data acquisition was carried out over seven sampling dates spanning the ripening period from veraison (BBCH 81: beginning of ripening, berries developing variety-specific colour) through commercial harvest (BBCH 89: berries ripe for harvest) (Lorenz *et al.*, 1995). Sampling commenced on 5 August 2025 and continued at approximately weekly intervals (12 August, 18 August, 25 August, 1 September, 8 September) until harvest on 15 September 2025, at the discretion of the vineyard manager, once the grapes reached optimal ripeness (approximately 23 °Brix). This temporal framework enabled the collection of samples exhibiting a wide range of maturity conditions, essential for the development and training of robust predictive models.

Sampling was conducted within a predefined experimental area comprising five central rows of the vineyard plot. On each sampling date, between 15 and 20 consecutive vines were

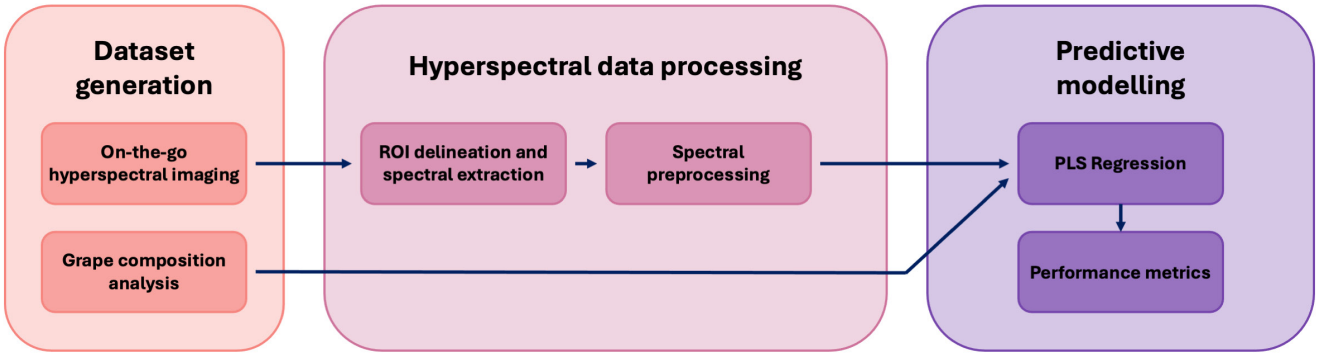


FIGURE 1. Main stages of the experimental workflow, from hyperspectral image acquisition to predictive model development.

assessed sequentially along the rows. The term "consecutive" refers to their spatial continuity; however, occasional gaps corresponding to missing or severely damaged vines were excluded to ensure sample representativeness. The exact number of vines sampled per date varied depending on vine productivity and the total berry mass required for the complete analytical panel.

Following hyperspectral imaging, grape clusters were destructively harvested from the scanned vines, so on subsequent sampling dates, measurements were performed on a new set of vines, continuing sequentially from the position where the previous session ended. When the end of a row was reached, sampling moved to the next adjacent marked row within the predefined experimental area.

For each sampling session, basal leaf removal was performed manually in the fruiting zone prior to imaging. Basal leaf removal in the cluster region is a common viticultural practice employed to improve spray penetration, reduce disease pressure, and enhance fruit exposure (Poni *et al.*, 2006), whilst also preventing cluster occlusion during imaging acquisition, which would otherwise compromise the quality and consistency of hyperspectral data.

2. Hyperspectral data collection

2.1. Image acquisition

Hyperspectral images were acquired on-the-go between 10:00 and 12:00 solar time, using a modified brushcutter AS 940 XL Sherpa 4WD (AS-Motor, Germany) equipped with a hydrostatic variator maintaining constant speeds of 1–3 km h^{-1}. The following two pushbroom hyperspectral cameras (Resonon Inc., Bozeman, MT, USA) were mounted on the platform and connected to an industrial computer (Figure 2): i) a Pika L camera covering the VIS-NIR range (400–1000 nm, 281 bands, 2.7 nm spectral resolution, 900 spatial pixels), equipped with an 8.0 mm focal length lens (f/1.4, 36.5 ° field of view), and positioned at 1.0 m from the target canopy, and ii) a Pika IR camera covering the SWIR range (900–1700 nm, 168 bands, 8.8 nm spectral resolution, 320 spatial pixels), equipped with a 25 mm focal length lens (f/1.8, 21.7 ° field of view), and positioned at 1.5 m from the target. Both cameras were oriented perpendicular to the row direction, providing a lateral point of view of the canopy. At the selected working distances, the resulting scan lines covered approximately 66 cm (Pika L) and 57 cm (Pika IR) of canopy height, ensuring full coverage of the fruiting zone (Figure 2). The camera-to-canopy distances were chosen so that five pixels of the Pika L camera approximately corresponded to two pixels of the Pika IR camera, facilitating subsequent spatial alignment between the VIS-NIR and SWIR data.

Imaging was conducted on the north-facing side of the canopy under natural sunlight conditions, supplemented with four 50 W vertical tungsten halogen lamps mounted vertically on the platform to provide additional and consistent illumination along the vertical line captured by the pushbroom sensors.

On each imaging session, camera settings were fine-tuned according to ambient light conditions: integration times were set close to the maximum values allowed by the respective frame rates (30 fps for the Pika L and 60 fps for the Pika IR) in order to achieve an optimal trade-off between acceptable image composition, adequate signal-to-noise ratio, and avoidance of pixel saturation.

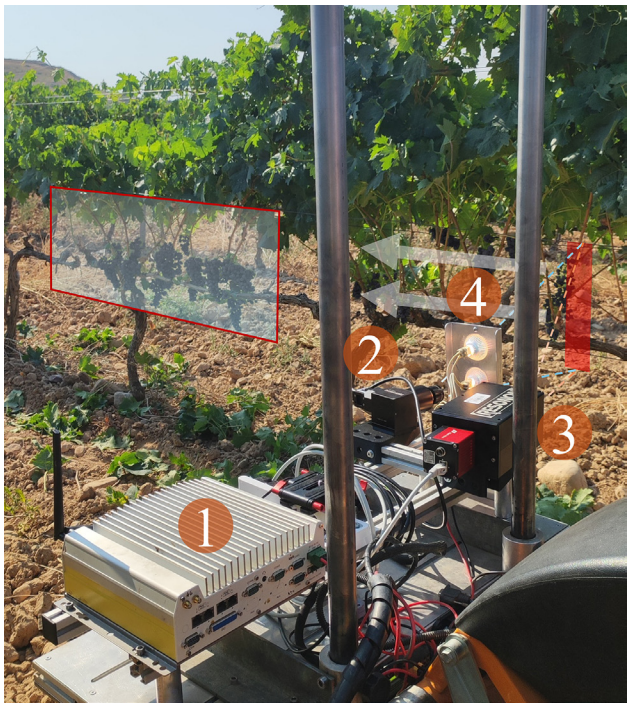


FIGURE 2. On-the-go HSI acquisition setup.

Industrial computer (1), Pika L (2), and Pika IR (3) hyperspectral cameras mounted on either side of the halogen illumination system (4) installed on a mobile platform.

Before each acquisition run, radiometric calibration was performed using a Spectralon® white reference panel (> 95 % reflectance across the spectral range) and dark current measurements obtained by blocking the camera lenses. Relative reflectance was then derived from the raw sensor output according to Equation 1:

$$R_\lambda = \frac{S_\lambda - D_\lambda}{W_\lambda - D_\lambda} \qquad \text{(Equation 1)}$$

where R_λ is the relative reflectance at wavelength λ, S_λ is the raw sensor signal from the target, D_λ is the dark current, and W_λ is the white reference signal at the same wavelength. This calibration procedure converts raw digital numbers into relative reflectance values, normalising variations in sensor response and illumination conditions.

2.2. Spectral data extraction and preprocessing

Hyperspectral images were processed using Spectronon® software (v3.5.8, Resonon Inc., Bozeman, MT, USA). On each date, one or two hyperspectral images encompassing the set of selected vines were acquired. These full-scene images were subsequently cropped to generate individual vine-level sub-images. This stepwise image handling ensured a consistent spatial framework for subsequent spectral extraction while preserving the original acquisition geometry.

Within each sub-image, grape cluster regions of interest (ROI) were manually delineated to isolate berry surfaces from background elements such as leaves, stems, soil, and shaded areas (Figure 3).

This manual segmentation ensured that only spectral information from grape berries was retained for subsequent analysis. Following ROI delineation, the mean reflectance spectrum of each ROI was computed and used as the representative spectral signature for that sample. This averaging process is a common approach in hyperspectral studies of fruit and grape composition, as it reduces pixel-level noise and local variability while preserving the overall spectral signature associated with berry maturity (Fernández-Novales *et al*., 2021). Figure 3 illustrates this process, displaying a pseudo-RGB reconstruction of the hyperspectral image, the delineated mask of the selected ROI, and the resulting mean spectral signature.

Following spectral extraction, a series of pre-processing techniques was applied prior to chemometric analysis. Spectral pre-processing is a critical step in reflectance spectroscopy, as raw spectra often contain variability unrelated to the chemical composition of the sample. According to Barnes *et a*l. (1989), spectral variation arises from three main sources: non-specific scatter of radiation at particle surfaces, variations in optical path length, and the intrinsic chemical composition of the sample. Pre-processing methods are therefore employed to reduce these unwanted effects, improve signal-to-noise ratio, and enhance the interpretability and robustness of subsequent multivariate models (Amigo *et al*., 2013).

In this study, combinations of several pre-processing techniques were evaluated, including Standard Normal Variate (SNV), detrending (DT), Savitzky-Golay (SG) smoothing and derivative transformations, and mean centring (MC). These methods were selected based on their widespread use in chemometric applications involving grape and fruit spectroscopy, as well as their proven effectiveness in correcting scatter effects and baseline variations (Rinnan *et al*., 2009).

SNV was applied on a spectrum-by-spectrum basis to correct for multiplicative scatter effects and differences in optical path length by scaling each spectrum to zero mean and unit variance (Barnes *et al*., 1989). This transformation is particularly effective when analysing samples measured under variable illumination conditions or with heterogeneous surface properties, as is often the case in field-based hyperspectral measurements. Detrending was evaluated in conjunction with SNV to remove residual baseline curvature by fitting and subtracting a second-order polynomial. Savitzky-Golay derivatives were employed to perform simultaneous smoothing and differentiation using local polynomial regression within a moving window, reducing baseline offsets whilst enhancing subtle absorption features associated with grape composition (Savitzky & Golay, 1964; Brown *et al.*, 2000). In this study, SG derivatives were computed using second-order polynomials with window sizes ranging from 5 to 19 data points. Finally, mean centring was performed prior to modelling by subtracting the average spectrum from each individual spectrum, thereby focusing the analysis on variance around the mean rather than absolute signal magnitude.

3. Grape composition analysis

Immediately after imaging, all grape clusters from each vine were manually harvested and transported under refrigerated conditions to the Institute of Grapevine and Wine Sciences (ICVV, Logroño, Spain).

For the analysis of total soluble solids, pH, titratable acidity, yeast-assimilable nitrogen, malic acid, tartaric acid, and anthocyanins, a random subsample of 200 berries (per vine sample) was handselected from each pooled sample, manually crushed, and the resulting must was strained and centrifuged at 12,000 rpm for 8 min at 4 °C using a Sorvall Lynx 4000 centrifuge (Thermo Fisher Scientific Inc., Waltham, MA, USA).

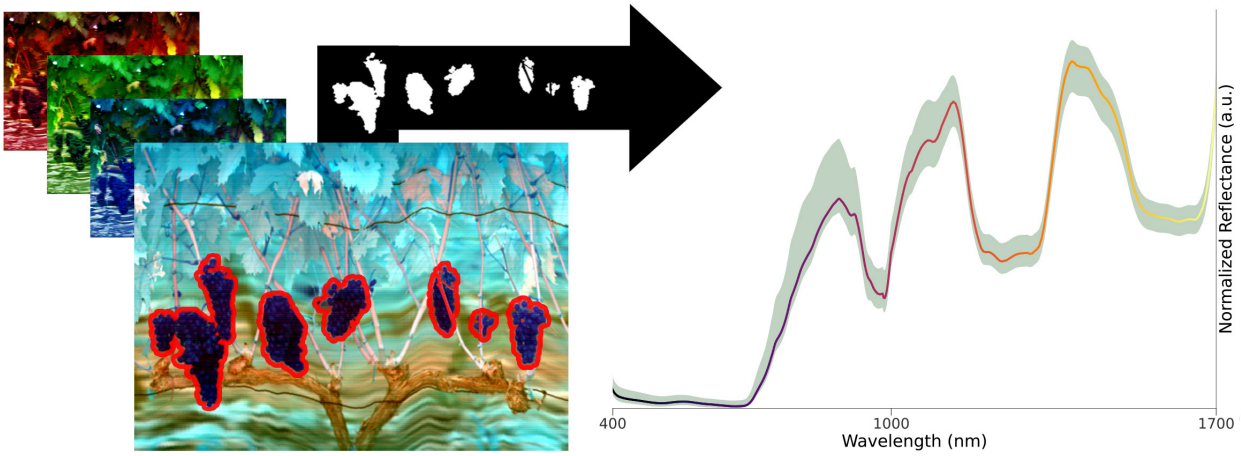


FIGURE 3. Workflow of the extraction of average grape berry spectra from hyperspectral images.

From left to right: pseudo-RGB reconstruction using three near-infrared bands mapped to RGB, followed by a binary ROI mask isolating berry pixels, and the corresponding mean reflectance spectra over the 400–1700 nm range. Shaded areas indicate the variability of ROI-averaged spectra for the same sampling date.

TSS, pH, and TA were determined using conventional OIV methods (OIV, 2024). TSS were measured using a temperature-compensating digital refractometer (Quick-Brix 60, Mettler Toledo, Columbus, OH, USA), and pH was determined with a benchtop pH meter (PH 8 PRO, XS Instruments, Codogno, Italy). TA was determined by titration with 0.1 N sodium hydroxide using bromothymol blue as indicator and expressed as g L^{-1} tartaric acid equivalents.

MH_2, TH_2, anthocyanins, and YAN were quantified using an enzymatic multiparameter analyser with commercial reagent kits (BioSystems Y-200, Barcelona, Spain).

While technological parameters and anthocyanins were determined on fresh berries, grape clusters intended for the remaining phenolic determinations were stored at –20 °C immediately after imaging. Prior to extraction, samples were allowed to thaw overnight at 4 °C in a cold room.

For spectrophotometric phenolic determinations, a separate wine-like extraction procedure was applied based on the methodological principles established by Glories (1984) and Iland *et al.* (2004), adapted to better reflect red winemaking conditions typical of Rioja.

Three independent replicates of 100 g of berries from each sampled vine were homogenised for 15 s at speed 1 using a 1000 W hand-held blender Moulinex DD65A810 QuickChef (Moulinex, Écully, France) to disrupt skin and pulp tissues whilst maintaining seed integrity. An equal mass (100 g) of hydroalcoholic extraction medium (14 % vol. ethanol, 5 g L^{-1} tartaric acid, pH adjusted to 2.0 with HCl) was then added to the homogenate. This extraction medium was designed to enhance phenolic solubilisation through acidification, while representing an intermediate between typical fermentation pH and the strongly acidic conditions used to estimate maximum extractability (Lorrain *et al*., 2013). The addition of 14 % (*v/v*) ethanol further contributes to mimicking the polarity and solvent properties of a fermenting red must-wine system, thereby enhancing the relevance of the extracted phenolic profile to practical winemaking conditions (Canals *et al*., 2005).

Following a 4 h extraction period at room temperature with periodic agitation, samples were strained and centrifuged at 10,000 rpm for 10 min at 4 °C using the same Sorvall Lynx 4000 centrifuge.

It is important to note that the phenolic extraction protocol was designed to maximise solubilisation of skin-derived phenolic compounds whilst minimising seed tannin release. Although seeds contribute significantly to wine phenolic composition and mouthfeel perception (Garrido & Borges, 2013), seed-derived tannins remain largely undetectable by hyperspectral reflectance measurements due to limited light penetration into the berry interior (few mm), with spectral sensitivity predominantly confined to skin surface composition.

The resulting grape extracts were analysed spectrophotometrically using a UV-Vis spectrophotometer (Agilent Cary 60, Agilent Technologies, Santa Clara, CA, USA), and results were expressed as the mean of the three independent extractions. TPI was determined as absorbance at 280 nm following 1:50 dilution in distilled water. CI was calculated as the sum of absorbances at 420, 520, and 620 nm according to Equation 2:

$$CI = A_{420} + A_{520} + A_{620} \qquad \text{(Equation 2)}$$

Additionally, to provide a more complete characterisation of extract colour properties, CIELab colour coordinates (L^*, a^*, b^*) were determined from the transmission spectra (380–780 nm) considering the CIE standard illuminant D65 and the 10 ° standard observer. In this colour space, L^* represents lightness (0 = black, 100 = white), a^* represents the red-green axis (positive values indicate red, negative values indicate green), and b^* represents the yellow-blue axis (positive values indicate yellow, negative values indicate blue).

Aliquots of the wine-like extracts were frozen at −20 °C for subsequent phenolic profiling by UHPLC/QqQ-MS/MS.

4. Model building and validation

Partial least squares regression (PLSR) was employed to develop quantitative predictive models relating hyperspectral reflectance data to grape composition parameters. PLSR models were trained in MATLAB R2016b (MathWorks Inc., Natick, MA, USA) using PLS-Toolbox v8.1 (Eigenvector Research Inc., Manson, WA, USA).

PLSR is a widely adopted chemometric technique in spectral analysis due to its ability to handle datasets where the number of predictor variables (wavelengths) significantly exceeds the number of samples, and where high multicollinearity exists among these predictors (Wold *et al*., 2001).

Unlike ordinary multiple linear regression, PLSR decomposes both the predictor matrix (X, spectral data) and the response matrix (Y, grape composition parameters) into a reduced set of orthogonal latent variables (LVs) that capture the maximum covariance between X and Y. This latent variable framework allows effective dimensionality reduction while retaining the spectral information most relevant for predicting the response variables, thereby improving model robustness in the presence of noise and multicollinearity (Helland, 2001).

With the aim of building robust models with adequate generalisation capacity, the original dataset of 110 samples was split into two independent datasets: a calibration set comprising 80 % of the samples (n = 90) and an independent prediction set with the remaining 20 % (n = 20) (Table 1).

Sample allocation to each subset followed a stratified partitioning strategy designed to ensure representativeness across both temporal and compositional variability. Stratification was performed in two steps: (i) temporal stratification, ensuring that at least two vines from each of the seven sampling dates were represented in both subsets; and (ii) compositional stratification, ensuring that the full range of variation for each target parameter was covered by allocating samples from each quartile of the ranked concentration distribution to both calibration and prediction groups. This

approach guaranteed that both subsets exhibited comparable statistical distributions and overlapping concentration ranges across all measured parameters (Table 1).

PLSR models were constructed from the calibration set, with adequate model complexity determined via 10-fold Venetian blind cross-validation. In this procedure, the calibration samples are divided into ten segments, with nine segments used iteratively for model training whilst the remaining segment is used for performance evaluation. By rotating through all ten segments, each sample is predicted once without being included in the corresponding training subset. Cross-validation statistics thus provide an unbiased estimate of model performance and help prevent overfitting whilst guiding the selection of the optimal number of latent variables.

Following model optimisation, the final PLSR models were evaluated on the independent prediction set to assess their true predictive ability on completely unseen samples that played no role in either model training or parameter selection.

Model performance was evaluated using the coefficient of determination (R^2) and the root mean square error (RMSE), which are among the most widely adopted metrics for assessing regression models in chemometrics. The coefficient of determination (R^2) quantifies the proportion of variance in the reference measurements explained by the model, with values closer to 1 indicating stronger predictive ability. It is defined as Equation 3:

$$R^2 = 1 - \frac{\sum_{i=1}^{n}(y_i - \hat{y}_i)^2}{\sum_{i=1}^{n}(y_i - \bar{y})^2} \qquad \text{(Equation 3)}$$

where y_i are the measured reference values, $\hat{y}_i$ are the corresponding model predictions, and $\bar{y}$ is the mean of the measured values.

The root mean square error (RMSE) provides an absolute measure of prediction accuracy by quantifying the average magnitude of the residuals between predicted and measured values, and is expressed as Equation 4:

$$RMSE = \sqrt{\frac{1}{n}\sum_{i=1}^{n}(y_i - \hat{y}_i)^2} \qquad \text{(Equation 4)}$$

Lower RMSE values indicate improved model accuracy and reduced prediction error and is expressed in the same units as the original reference parameter.

For each PLS model, the optimal number of LVs was selected as the one minimising the root mean square error of cross-validation (RMSECV), thereby avoiding overfitting while maximising predictive performance. Model quality was assessed at three different stages: calibration (R^2_c, RMSEC), cross-validation (R^2_{cv}, RMSECV), and independent prediction (R^2_p, RMSEP). The combination of these metrics allowed a comprehensive evaluation of model robustness, generalisation capability, and predictive reliability when applied to unseen samples.

RESULTS

1. Grape compositional dynamics

Descriptive statistics for all grape composition parameters across the complete dataset and its calibration and independent prediction subsets are presented in Table 1.

TSS increased from 13.9 to 24.5 °Brix, pH values ranged from 2.75 to 4.16, and correspondingly, TA decreased from 19.35 to 3.30 g L^{-1}, driven primarily by a pronounced decline in MH_2. In contrast, TH_2 remained relatively stable, consistent

TABLE 1. Descriptive statistics of cv. Tempranillo berry composition.

	Data set			Calibration set			Independent prediction set		
Parameter	Range	Mean	SD	Range	Mean	SD	Range	Mean	SD
TSS (°Brix)	13.9-24.5	20.4	2.9	13.9-24.5	20.4	2.9	13.9-23.9	20.7	2.9
pH	2.75-4.16	3.52	0.38	2.77-4.16	3.52	0.38	2.75-4.10	3.51	0.38
TA (g L^{-1})	3.30-19.35	6.96	4.47	3.30 - 19.35	6.84	4.39	3.38-18.82	7.48	4.91
TH2 (g L^{-1})	3.13-7.03	4.77	0.97	3.13-7.03	4.76	0.99	3.33-6.80	4.80	0.92
MH2 (g L^{-1})	1.62-11.30	3.89	2.69	1.62-11.30	3.79	2.60	1.93-10.98	4.33	3.06
YAN (mg L^{-1})	99-788	311	120	99-788	311	125	168-549	313	95
Anth. (mg L^{-1})	9-237	44	40	10-237	44	40	9-182	44	40
TPI (AU)	30.07-79.42	47.27	9.36	30.53-79.42	47.40	9.57	30.07-65.68	46.66	8.63
CI (AU)	5.15-27.14	16.08	5.79	5.15-27.14	16.23	5.89	5.24-24.03	15.43	5.41
CIELab L*	61.04-87.87	72.86	6.69	61.04-87.87	72.61	6.76	63.87-84.97	73.99	6.44
CIELab a*	15.55-47.84	35.20	8.32	15.55-47.84	35.37	8.41	15.55-44.91	34.42	8.07
CIELab b*	–0.71-4.56	1.39	1.31	–0.71-4.56	1.33	1.27	–0.19-4.56	1.64	1.50

TSS: total soluble solids; TA: titratable acidity (expressed as tartaric acid equivalents); TH_2: tartaric acid; MH_2: malic acid; YAN: yeast-assimilable nitrogen; Anth.: anthocyanins; TPI: total phenolic index; CI: colour intensity; AU: absorbance units; SD: standard deviation. The complete dataset comprised 110 samples, partitioned into calibration (n = 90) and independent prediction (n = 20) sets. For TPI, the first sampling date (n = 20) was excluded from the dataset due to anomalously high values attributed to methodological artefacts during sample preparation.

with established patterns of organic acid metabolism during maturation (Iland *et al.,* 2024). YAN also exhibited substantial variability (99–788 mg L^{-1}), indicating heterogeneous nitrogen status across sampling dates and individual vines.

Phenolic and colour-related parameters displayed wide ranges as well, reflecting progressive accumulation from veraison onwards. A critical methodological distinction must be noted: whilst anthocyanin concentration was determined on must obtained from manually crushed berries – representing extractability under mechanical pressing conditions – the remaining phenolic and colour parameters (TPI, CI, and chromatic coordinates) were measured on hydroalcoholic acidified extracts (pH 2.0, 14 % *v/v* ethanol) designed to enhance phenolic extraction and simulate conditions closer to those occurring during red wine maceration. This approach resulted in notably elevated values for TPI (30.07–79.42 AU) and CI (5.15–27.14 AU) compared to those reported for grape homogenates (Aleixandre-Tudo *et al.,* 2018), reflecting the phenolic potential that would be released from these grapes under winemaking conditions.

CIELab colour coordinates further characterised chromatic evolution, with positive a^* and low b^* values consistent with red pigmentation predominance, whilst L^* variation reflected differences in extract colour density.

Importantly, samples from the first sampling date (n = 20, shortly after veraison) were excluded from the TPI dataset due to anomalously high values inconsistent with the expected maturity stage. These aberrant values were attributed to methodological artefacts during sample preparation, likely resulting from non-uniform thawing or excessive seed disruption during homogenisation due to the smaller berry size and higher seed-to-pulp ratio characteristic of early veraison berries, which would have caused atypical tannin release. Consequently, excessive seed tannin extraction may introduce compositional variance unrelated to the spectral features captured by the imaging system, thereby weakening model performance. Particular attention should therefore be given in future studies to refining phenolic extraction protocols with the aim of minimising seed interference whilst maximising the alignment between spectral measurements and wine-relevant skin phenolic fractions.

Overall, sampling across the ripening period (BBCH 81–89) captured wide compositional variability for all parameters, which were associated with high standard deviations, thus providing favourable conditions for developing robust predictive models. The calibration and independent prediction sets exhibited comparable statistical distributions (Table 1), ensuring adequate representation of the compositional space and reliable assessment of model generalisation capacity.

2. Hyperspectral data analysis

Table 2 summarises the optimal spectral preprocessing method and number of latent variables selected for each grape composition parameter. The number of LVs reflects the spectral complexity of each trait: constituents with distinct absorption features generally require fewer LVs, whereas parameters with broader or overlapping spectra demand higher model dimensionality.

The preprocessing strategies employed combinations of Standard Normal Variate, detrending, Savitzky-Golay derivatives, and mean centring to minimise spectral artefacts and enhance model performance. Different preprocessing combinations were optimal for different parameters, reflecting the diverse spectral signatures and concentration ranges of grape constituents.

SNV and DT were universally applied across all models to correct for multiplicative scatter effects and baseline drift. For most parameters, first-derivative preprocessing (D1) was employed with varying window sizes (W5 to W19), effectively removing residual baseline variations whilst enhancing spectral features. Second-derivative preprocessing (D2) was selected for tartaric acid and malic acid models, which may reflect the need for enhanced resolution of overlapping absorption bands in the carboxylic acid spectral region. Notably, the CIELab L^* model uniquely employed no derivative transformation (D0W15). This preprocessing choice is physically consistent with the nature of the L^* parameter: lightness represents the overall magnitude of reflected signal, whereas derivative transformations emphasise localised spectral features. MC was applied to the majority of models to improve interpretability and numerical stability during PLS decomposition.

Figure 4 illustrates the raw hyperspectral reflectance spectra of all grape samples alongside the corresponding spectra after preprocessing using the SNV/DT/SGD1W15/MC combination. As observed, all spectral curves exhibited consistent morphology, indicating a qualitative similarity in the biochemical matrix across the dataset. However, significant variations in reflectance magnitude were evident among samples; these fluctuations in intensity are attributable to differences in the quantitative abundance of internal metabolites (*e.g.*, sugars, organic acids, and pigments) driven by the maturation process.

Crucially, the raw spectra exhibited substantial variability in overall intensity and baseline offset across samples, reflecting differences in illumination conditions, surface scattering, and sample geometry during on-the-go acquisition. In the short-wave infrared region, pronounced absorption features were evident, associated with water, sugars, and organic compounds, but these were partially masked by baseline drift and multiplicative effects in the unprocessed data.

After preprocessing, spectral baselines were effectively centred and normalised, substantially reducing inter-sample scattering effects while enhancing subtle absorption features across the full spectral range. The application of the first Savitzky-Golay derivative emphasised local spectral variations and resolved overlapping bands, particularly in the NIR-SWIR region, while suppressing low-frequency background trends. As a result, the preprocessed spectra exhibited improved alignment and comparability among samples, facilitating the extraction of chemically relevant information for subsequent multivariate modelling.

TABLE 2. Calibration, cross-validation, and independent prediction performance of the best PLS regression models for predicting grape composition from on-the-go hyperspectral imaging.

			Calibration		Cross-validation		Independent prediction	
Parameter	Spectral treatment	LVs	R^2_c	RMSEC	R^2_{cv}	RMSECV	R^2_p	RMSEP
TSS (°Brix)	SNV/DT/D1W7/MC	9	0.90	0.891	0.85	1.098	0.94	0.703
pH	SNV/DT/D1W15	4	0.93	0.099	0.92	0.106	0.93	0.099
TA (g L^{-1})	SNV/DT/D1W5	6	0.96	0.843	0.95	0.957	0.98	0.920
TH2 (g L^{-1})	SNV/DT/D2W17	6	0.84	0.399	0.80	0.444	0.79	0.450
MH2 (g L^{-1})	SNV/DT/D2W15/MC	5	0.94	0.623	0.92	0.710	0.95	0.782
YAN (mg L^{-1})	SNV/DT/D1W15/MC	8	0.76	61.249	0.67	71.531	0.56	74.083
Anth. (mg L^{-1})	SNV/DT/D1W15/MC	4	0.64	23.829	0.57	25.922	0.58	25.621
TPI (AU)	SNV/DT/D1W19/MC	5	0.78	4.487	0.73	4.988	0.76	4.230
CI (AU)	SNV/DT/D1W13/MC	7	0.92	1.660	0.90	1.889	0.88	2.058
CIELab L*	SNV/DT/D0W15/MC	5	0.87	2.427	0.85	2.559	0.81	3.195
CIELab a*	SNV/DT/D1W13/MC	7	0.89	2.785	0.86	3.104	0.88	3.031
CIELab b*	SNV/DT/D1W15/MC	7	0.87	0.452	0.83	0.517	0.89	0.532

TSS: total soluble solids; TA: titratable acidity (expressed as tartaric acid equivalents); TH_2: tartaric acid; MH_2: malic acid; YAN: yeast-assimilable nitrogen; Anth.: anthocyanins; TPI: total phenolic index; CI: colour intensity; AU: absorbance units. SNV: Standard Normal Variate; DT: Detrending; DnWm: Savitzky-Golay filter with n-degree derivative, window size of m; MC: Mean Centring. LVs: Latent variables. R^2_c: determination coefficient of calibration; RMSEC: root mean square error of calibration; R^2_{cv}: determination coefficient of cross-validation; RMSECV: root mean square error of cross-validation; R^2_p: determination coefficient of prediction; RMSEP: root mean square error of prediction.

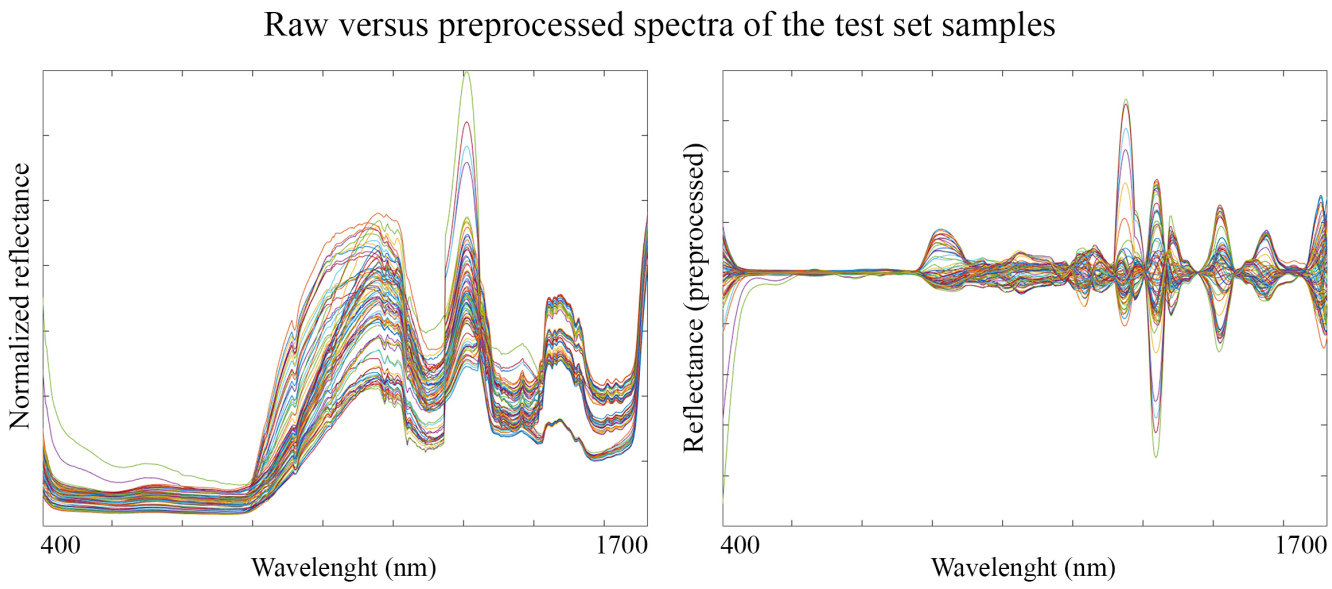


FIGURE 4. Effect of spectral preprocessing on grape hyperspectral data (test set).

Average grape bunch reflectance spectra normalised against a Spectralon® reference (left) and the corresponding preprocessed spectra after application of the selected preprocessing pipeline (right), including Standard Normal Variate (SNV), detrending, and Savitzky-Golay filtering. Spectral range: 400–1700 nm.

The number of latent variables ranged from 4 (pH and anthocyanins) to 9 (TSS), indicating varying degrees of spectral complexity required to capture each parameter's relationship with the hyperspectral data. Parameters related to sugar content (TSS, 9 LVs) and nitrogen status (YAN, 8 LVs) required the highest model dimensionality, likely due to their spectral signatures involving multiple overlapping absorption bands distributed across both VIS-NIR and SWIR regions associated with C–H, O–H, and N–H bond overtones (Williams & Norris, 2001; ElMasry & Sun, 2010). Conversely, pH and anthocyanins achieved adequate predictive performance with only 4 LVs. Anthocyanins exhibit well-defined absorption features in the visible region, with characteristic peaks around 520–530 nm (Agati *et al*., 2007), whilst organic acids show localised spectral signatures in both visible and near-infrared regions, potentially explaining the lower model complexity for these parameters. Colour-related parameters (CI, CIELab *L**, *a**, and *b**) required 5–7 LVs, whilst phenolic indices (TPI) and acids (TH_2, TA, MH_2) employed 5–6 LVs. The selection of optimal LV numbers through cross-validation ensured a balance between model complexity and generalisation capacity, avoiding overfitting whilst capturing the essential variance in both spectral and compositional data.

3. Predictive model performance

Table 2 summarises the statistical performance of the PLS regression models, detailing metrics for calibration (R^2_c, RMSEC), cross-validation (R^2_{cv}, RMSECV), and external prediction (R^2_p, RMSEP), which collectively evaluate the predictive capacity of the models on both calibration samples and previously unseen data. Overall, the models demonstrated varied predictive performance across the different grape composition parameters, with calibration fits (R^2_c) ranging from 0.64 to 0.96, that were consistently maintained through cross-validation and independent prediction, supporting their reliable predictive ability on unknown samples under field conditions.

According to the classification criteria proposed by Shenk and Westerhaus (1995), models achieving $R^2 \geq 0.90$ provide excellent quantitative information, whereas values between 0.70 and 0.89 indicate good quantitative prediction. Intermediate R^2 values (0.50–0.69) are considered suitable for reliably separating samples into high, medium, and low concentration groups, while lower ranges (0.30–0.49) allow discrimination between high and low values only; $R^2 \leq 0.29$ provides no meaningful predictive information.

Figure 5 illustrates the predictive performance of the PLS models on the independent test set. All evaluated parameters demonstrated robust predictive capacity, with R^2_p values exceeding 0.56. The predictions were consistently distributed around the 1:1 line, confirming the models' generalisation ability on hold-out samples.

Excellent predictive performance was obtained for total soluble solids, titratable acidity, pH, and malic acid. In particular, TA and MH_2 achieved the highest external determination coefficients (R^2_p = 0.98 and 0.95, respectively), and also a substantially narrow confidence interval, highlighting the effectiveness of hyperspectral data in capturing organic acid-related absorption features and the robustness of the developed models under the conditions of this study. Similarly, TSS (R^2_p = 0.94) and pH (R^2_p = 0.93) also fell within the range of excellent quantitative information, with remarkably low RMSEP values (0.703 °Brix and 0.099, respectively). The colour-coded distribution in Figures 5a, 5b, 5c, and 5e illustrates the expected temporal evolution of maturity. Specifically, TA and MH_2 exhibit a progressive decrease from veraison to harvest, whereas TSS and pH show a concurrent increase. These trends accurately reflect the typical metabolic shifts occurring during berry ripening, which ultimately determine the potential alcohol content and acid balance of the resulting wine.

In contrast, tartaric acid exhibited good performance (R^2_p = 0.79, RMSE = 0.450 g L^{-1}), though slightly below the threshold for excellent quantitative prediction. Figure 5d confirms the robustness of the model, with predictions closely following the 1:1 line across the concentration range. However, a noticeably wider confidence interval compared to MH_2 can be observed, and the model showed a discernible accuracy loss from the calibration phase (R^2_c = 0.84) to independent prediction. This behaviour likely reflects the relative stability of TH_2 during ripening, which leads to a narrower concentration range and weaker spectral variability relative to MH_2, thereby limiting modelling accuracy due to potential spectral overlapping with other organic acids. Despite these constraints, the model retains practical utility for monitoring TH_2 levels during grape maturation.

YAN displayed limited predictive performance (R^2_p = 0.56, RMSE = 74.083 mg L^{-1}), with substantial degradation from calibration (R^2_c = 0.76) to independent prediction. A notably broader confidence interval is observed compared to other parameters, particularly driven by several outlying points from the fourth and especially the fifth sampling dates (Figure 5f). Despite the elevated prediction error, the model clearly captures the overall trend, following the 1:1 relationship across the concentration range. This modest accuracy falls below the threshold for reliable quantitative prediction, though it may still provide approximate screening capacity for distinguishing samples with high, medium, or low nitrogen status. The limited predictive capacity may reflect the chemical complexity of nitrogen compounds in grapes, which encompass diverse forms (ammonium ions, free amino acids, peptides) with potentially overlapping spectral signatures in the VIS-NIR-SWIR range, as well as the substantial spatial and temporal heterogeneity observed for this parameter (CV = 38.5 %).

Phenolic and colour parameters achieved varied predictive performance. TPI achieved good quantitative prediction (R^2_p = 0.76, RMSE = 4.230 AU). Anthocyanins showed more modest results (R^2_p = 0.58, RMSE = 25.488 mg L^{-1}), enabling approximate separation into concentration groups. Finally, colour-related parameters demonstrated strong performance: CI (R^2_p = 0.88, RMSE = 2.058 AU), CIELab *L** (R^2_p = 0.81, RMSE = 3.195), CIELab *a** (R^2_p = 0.88, RMSE = 3.031) and *b** (R^2_p = 0.89, RMSE = 0.532). Nevertheless, the strong

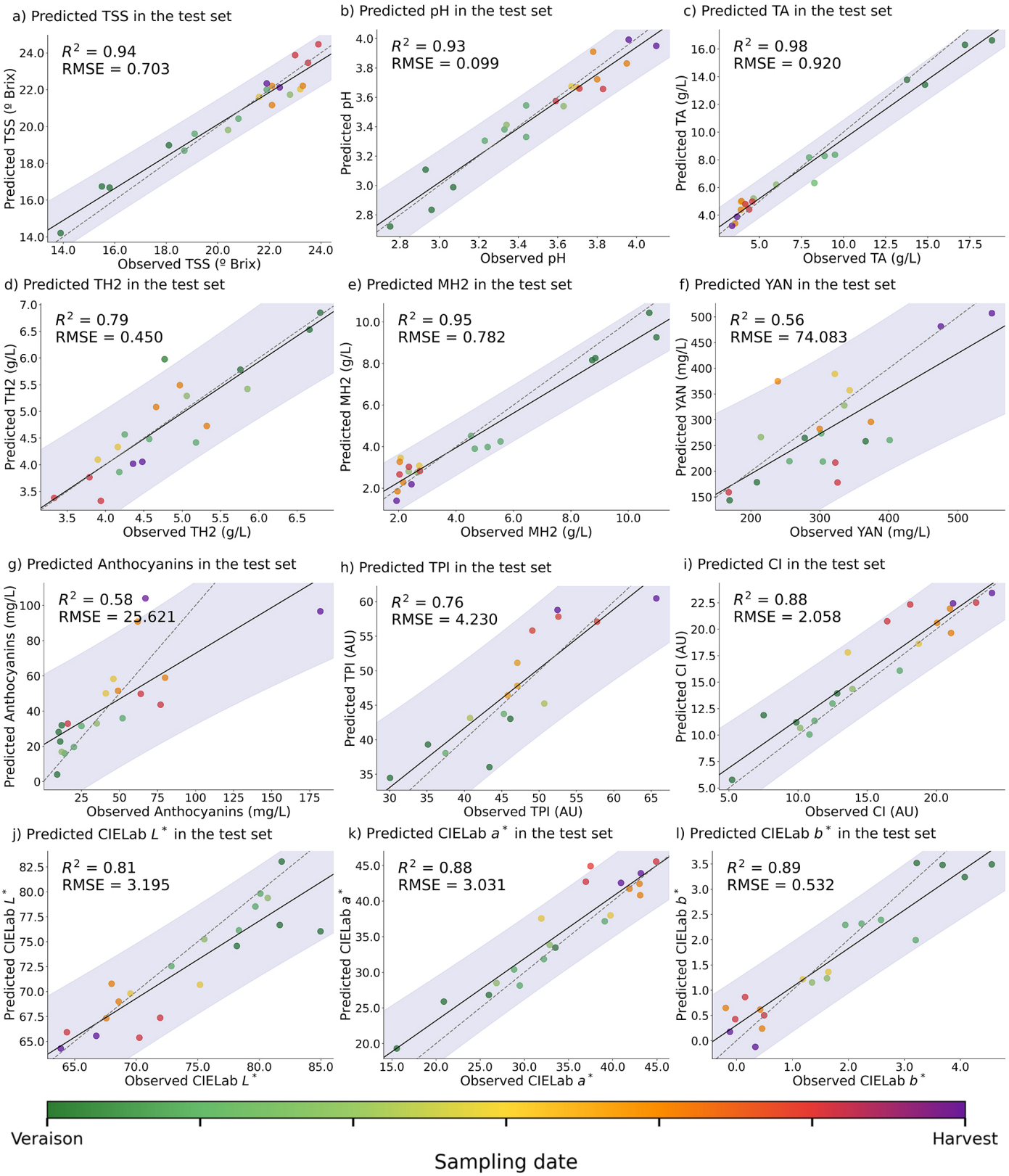


FIGURE 5. Observed versus predicted values for parameters in the external test set using PLS.

Each panel shows the determination coefficient (R^2_p) and root mean square error (RMSEP) for prediction. The dashed line represents the 1:1 relationship, and the shaded area indicates the 95 % confidence interval. Colour of data points represent sampling date. TSS: total soluble solids; TA: titratable acidity; TH_2: tartaric acid; MH_2: malic acid; YAN: yeast-assimilable nitrogen; Anth.: anthocyanins; TPI: total phenolic index; CI: colour intensity.

performance is consistent with the pronounced absorption features of phenolic compounds in the VIS region and justifies the use of hyperspectral imaging for objective colour characterisation of intact berries as a proxy for phenolic maturity.

Anthocyanin prediction warrants particular attention given its relevance for red wine quality. While the model achieves moderate predictive performance, sufficient for screening purposes, it exhibits substantially wider confidence intervals compared to other parameters (Figure 5g). The colour-coded distribution reveals the expected accumulation pattern during ripening, with anthocyanin content progressively increasing from veraison (green points) through intermediate stages (yellow-orange points) to harvest (red-purple points). However, considerable dispersion is observed, particularly at later sampling dates, where predictions range from approximately 45 to 105 mg L^{-1} for similar observed values. This behaviour partly reflects the substantial plant-to-plant variability in anthocyanin accumulation. Additionally, the relatively lower performance may be attributed to methodological differences, as anthocyanins were determined on fresh must whilst other phenolic parameters were measured on hydroalcoholic acidified extracts.

Remarkably, the statistical performance remained relatively consistent across the calibration, cross-validation, and independent prediction phases, confirming the representativeness of the calibration-validation split and the generalisation capacity of the models. Interestingly, in some cases the independent prediction error (RMSEP) was comparable to or even lower than the cross-validation error (RMSECV). This can be explained by the conservative nature of Venetian blinds cross-validation, which systematically tests the model against all folds, including those containing spectral outliers, whereas the independent prediction set had slightly narrower concentration ranges (Table 1), excluding extreme values that typically penalise performance. Consequently, the high accuracy achieved on this independent set indicates that the PLS models effectively captured the relevant chemical variance without overfitting, supporting their practical application for reliable, nondestructive, in-field assessment of key compositional traits that define harvest readiness and wine style in 'Tempranillo'.

It should be noted that some parameters exhibited uneven sample distributions across their respective concentration ranges, resulting in visible gaps in the scatter plots, particularly for MH_2, YAN, and anthocyanins (Figures 5e, 5f, and 5g, respectively). These discontinuities reflect the intrinsic compositional structure of the dataset, which is shaped by ripening-stage clustering and the limited number of samples available for model evaluation, rather than indicating failure within specific intervals. Nevertheless, such gaps may influence the apparent stability of the regression line and limit the strength of inference for concentration ranges that are sparsely represented. In the case of MH_2, despite this non-uniform distribution, the low prediction error and strong agreement with the expected physiological decline during ripening support the robustness of the model within the sampled range. Future validation using larger datasets with more continuous coverage of intermediate and extreme values would help to further assess model generalisation across the full compositional spectrum.

DISCUSSION

Recently, hyperspectral imaging has demonstrated strong potential for non-destructive prediction of grape quality attributes, with laboratory studies frequently reporting R^2 values exceeding 0.80–0.90 for technological maturity parameters (Ye *et al*., 2023). Such environments typically represent a methodological baseline, which is characterised by stable diffuse illumination, absence of canopy interference, and optimal sample positioning – conditions that inherently minimise the spectral noise encountered during dynamic on-the-go scanning of whole bunches under variable field conditions. Consequently, contrasting these controlled experimental conditions with the present results is fundamental to assess the practical applicability of the proposed workflow.

Concerning technological maturity parameters, the models developed herein for TSS (R^2_p = 0.94, RMSEP = 0.70 °Brix), TA (R^2_p = 0.98, RMSEP = 0.92 g L^{-1}), and pH (R^2_p = 0.93, RMSEP = 0.099) achieved excellent predictive performance, with metrics that align with or favourably compare to those documented in the literature under laboratory scenarios. For instance, Gomes *et al.* (2017), trained PLS models to predict sugar content in whole Port 'Touriga Franca' wine grape berries using VIS-NIR imaging (380–1028 nm), reporting an RMSEP of 0.94 °Brix when testing on the same vintage (2012) and 1.34 °Brix for an independent year (2013). Baiano *et al*. (2012) applied a comparable spectral range to table grape cultivars including 'Italia' and 'Red Globe', achieving R^2_p values of 0.93–0.94 for TSS and 0.82–0.95 for TA and with varying performance depending on grape colour (superior accuracy in white cultivars). Similarly, Nogales-Bueno *et al*. (2014) documented higher correlations (R^2 = 0.97) for TSS in 'Tempranillo', 'Syrah', and 'Zalema' using NIR imaging (900–1700 nm), but their standard error of prediction (SEP = 1.61 °Brix) exceeded the RMSEP reported in the present study. In contrast, Piazzolla *et al.* (2017), working on fresh 'Italia' table grapes with a portable VIS-NIR device (400–1000 nm), reported considerably inferior coefficients of determination for both TA (R^2_p = 0.78) and pH (R^2_p = 0.70), attributing these lower correlations to the high variance within the juice of the 15-berry samples used as a reference.

Comparisons with recent advanced computational techniques further contextualise these findings. Gao and Xu (2022) achieved an R^2_p of 0.95 with a prediction error of 0.705 °Brix for TSS in 'Red Globe' grapes by fusing spectral data (391–1043 nm) with image texture features; meanwhile Xu *et al.* (2023) attained an R^2_p of 0.92 for TA when applying deep learning algorithms (Stacked Auto-Encoders) coupled with Least Squares Support Vector Machines (LSSVM) to hyperspectral images of 'Kyoho' grapes. Similarly, fusing spectral and image data, Gao and Xu (2024) reported a higher correlation (R^2_p = 0.99) in 'Red Globe' grapes, but with a slightly elevated prediction error (RMSEP = 1.07 g L^{-1})

relative to our results. Regarding pH, Gao and Xie (2024) reported an R^2_p of 0.96 using an IRIV-PLSR variable selection strategy in laboratory conditions, which closely aligns with our in-field result. Achieving comparable or superior accuracy using spectral information alone, with straightforward linear PLS regression and standard preprocessing, highlights the robustness of the proposed chemometric workflow and suggests that carefully calibrated linear models offer practical advantages in terms of computational cost, model interpretability, and operational simplicity – critical considerations for scalable vineyard deployment.

The determination of phenolic composition, however, proved more sensitive to the constraints of the experimental environment. For TPI, our model achieved R^2_p of 0.76 (RMSEP = 4.23 AU). While this performance falls below laboratory-based reports, such as Nogales-Bueno *et al*. (2014), who obtained $R^2 = 0.89$ on homogenised grape skins, or Gabrielli *et al.* (2023), who reported $R^2_p = 0.93$, it nonetheless demonstrates practical applicability for phenolic screening. In this context, our results align well with those documented by Khiari *et al.* (2025) for post-harvest raisins ($R^2 = 0.78$).

Anthocyanin prediction showed a more moderate performance ($R^2_p = 0.58$), which may be partly attributed to the use of fresh must reference values rather than skin extracts, introducing additional external variability. This outcome is consistent with previous reports highlighting the difficulty of anthocyanin estimation in intact berries; Fernandes *et al*. (2011), for example, reported a similar correlation ($R^2 = 0.65$) using complex adaptive neural network architectures under laboratory conditions, while standard PLS approaches performed poorly. Higher accuracies reported by Chen et al. (2015) ($R^2_p = 0.94$) relied on NIR spectral ranges and non-linear regression techniques (SVR). Nevertheless, the results obtained here support the suitability of VIS-NIR PLS models for categorical segregation of anthocyanin levels in field applications.

Chromatic parameters, closely linked to phenolic evolution, were predicted with particularly strong performance in the present work. CI reached an R^2_p of 0.88, exceeding values documented by Gabrielli *et al.* (2023) under laboratory conditions ($R^2_p = 0.81$). Furthermore, the present study successfully modelled the CIELab chromatic coordinates, enabling a multidimensional description of colour development during ripening. High predictive accuracy was achieved for lightness (L^*, $R^2_p = 0.81$) and both the red-green axis (a^*, $R^2_p = 0.88$) and the yellow-blue axis (b^*, $R^2_p = 0.89$). These results are competitive with those published by Khiari *et al.* (2025), who obtained R^2 values between 0.94 and 0.99 for L^*, a^*, and b^* using GAPLS variable selection, albeit on dried grapes in static laboratory conditions. A noteworthy difference between the present study and most of the existing literature in terms of methodology lies in the extraction protocol used for the reference phenolic analysis: in this work, the berries were extracted in a hydroalcoholic medium (14 % *v/v* ethanol, pH 2) to approximate wine-like conditions, whereas many laboratory studies relied on exhaustive skin extractions that quantify total phenolic reserves rather than extractable fractions (Nogales-Bueno *et al*., 2014; Chen *et al*., 2015).

Whilst laboratory-based studies provide essential information for evaluating sensor capabilities and calibration methodologies, the practical applicability of hyperspectral imaging for precision viticulture ultimately depends on performance under operational environments. Among the still limited body of literature addressing on-the-go hyperspectral imaging in commercial vineyards, the studies of Gutiérrez *et al*. (2019a) and Fernández-Novales *et al*. (2021) constitute the most relevant benchmarks, as both implemented pushbroom VIS-NIR systems mounted on all-terrain vehicles in *Vitis vinifera* L. cv. Tempranillo under real field conditions. Using single VNIR cameras (400–1000 nm), Gutiérrez *et al*. (2019a) reported determination coefficients of 0.92 for TSS and 0.83 for anthocyanins, while Fernández-Novales *et al*. (2021) (who were the first to extend on-the-go hyperspectral imaging to acidity-related parameters) obtained R^2_p values of 0.82 for TSS, 0.81 for TA, 0.61 for pH, 0.62 for TH_2, 0.84 for MH_2, 0.88 for anthocyanins, and 0.55 for total polyphenols. These pioneering studies demonstrated the feasibility of acquiring meaningful spectral information from grape clusters under uncontrolled vineyard conditions, establishing a methodological foundation for subsequent field-based work.

It is important to recognise, however, that direct numerical comparison of performance metrics across studies can be misleading, as the coefficient of determination depends strongly on the range of variability captured in each dataset. Similarly, differences in reference analytical protocols, sensor specifications, and preprocessing strategies complicate cross-study benchmarking. Consequently, whilst statistical metrics provide useful context, the practical utility of a prediction model is more meaningfully assessed by examining whether the prediction error is operationally acceptable for the intended decision-making context.

Within this framework, the on-the-go PLS models developed in the present study achieved competitive or superior performance across all evaluated parameters. For TSS, the prediction accuracy obtained here ($R^2_p = 0.94$, RMSEP = 0.703 °Brix) matches the correlation reported by Gutiérrez *et al.* (2019a), though with substantially lower prediction error (RMSEP = 1.274 °Brix), and represents an improvement over Fernández-Novales *et al*. (2021) (RMSEP = 1.22 °Brix). Likewise, Benelli *et al.* (2024), working in 'Sangiovese' vineyards with a manually pulled garden cart and advanced automatic ROI selection algorithms, reported a cross-validation R^2 of 0.74 (RMSE = 0.86 °Brix). Similarly, for acidity-related traits, TA ($R^2_p = 0.98$), pH ($R^2_p = 0.93$), and MH_2 ($R^2_p = 0.95$) models achieved higher accuracy compared to the more moderate performance reported by Fernández-Novales *et al*. (2021) ($R^2_p = 0.81$, 0.61, and 0.84, respectively). This enhanced performance highlights the added value of extending measurements into the SWIR range, where absorption features related to organic acids are more pronounced. From a viticultural perspective, this result is particularly relevant under warming scenarios, given the strong temperature sensitivity of malic acid during ripening.

It is also worth noting that linear PLS regression achieved competitive or superior performance compared to more complex computational approaches applied under field conditions. Using tripod-mounted snapshot hyperspectral imaging (400–1000 nm) combined with deep convolutional autoencoders for illumination correction, Tsakiridis *et al.* (2023) described prediction errors of RMSE = 1.6–2.29 °Brix, depending on the specific deep learning architecture employed.

Furthermore, the present study represents, to our knowledge, the first attempt to estimate yeast-assimilable nitrogen (YAN) from field-based hyperspectral data, achieving an R^2_p of 0.56; this opens up new avenues for supporting preliminary spatial stratification or informed decision-making regarding yeast nutrient supplementation during fermentation (Bell & Henschke, 2005). Whilst this performance is modest, it is comparable to challenges reported for other trace-level or chemically heterogeneous grape constituents. Marín-San Román *et al.* (2024) achieved cross-validation $R^2_{cv} \geq 0.5$ for individual volatile compounds in 'Tempranillo' berries under controlled laboratory conditions, yet external validation on independent samples showed substantial performance degradation for most analytes (*e.g.*, linalool R^2_p = 0.19, β-damascenone R^2_p = 0.005), with only (Z)-3-hexen-1-ol maintaining reasonable predictive capacity (R^2_p = 0.56). These findings illustrate that, even under optimal conditions, the prediction of low-concentration, spectrally overlapping compounds remains challenging when models are tested on truly independent datasets. Future research could explore whether targeting individual amino acids – rather than the aggregate YAN parameter – might yield improved prediction by exploiting more distinctive molecular signatures. Such an approach could benefit from expanded calibration datasets or the application of non-linear modelling architectures capable of resolving overlapping absorption bands.

Concerning phenolic compounds, the comparison with in-field studies reveals a stronger sensitivity to reference analytical protocols. Anthocyanin prediction in the present work (R^2_p = 0.58) was lower than the values documented by Gutiérrez *et al.* (2019a) and Fernández-Novales *et al.* (2021) (R^2_p = 0.83 and 0.88, respectively). However, this discrepancy is largely attributable to the previously discussed differences with laboratory-based literature in terms of the reference analysis: while those authors quantified anthocyanins on berry homogenates following the Iland method (Iland *et al.*, 2004), the present study determined anthocyanins in fresh must, providing complementary information on immediate pigment extractability under minimal mechanical disruption, which is analogous to the early stages of maceration. This approach, although relevant from a technological perspective, introduces additional variability associated with pigment release during crushing, which may reduce model performance. The lower correlation therefore likely reflects a mismatch between surface reflectance measurements and must-based reference values, rather than a limited sensitivity of the sensor to anthocyanin-related spectral features. This interpretation is supported by the high predictive accuracy achieved for colour intensity (R^2_p = 0.88), a parameter measured on acidified hydroalcoholic extracts that more directly reflects the overall phenolic potential of the grapes. Conversely, Bertoglio *et al*. (2024) reported lower anthocyanin prediction accuracy (R^2_{cv} = 0.49 at vine level) using snapshot imaging in table grapes, attributing this limitation to the heterogeneous spatial distribution of pigments within bunches and the weak correspondence between external reflectance and internal phenolic content.

Regarding alternative spectral acquisition modalities, snapshot hyperspectral systems have demonstrated potential for specific applications. Using a proximal snapshot camera (500–900 nm) combined with instance segmentation (Mask R-CNN), Bertoglio *et al.* (2024) observed R^2_{cv} values of 0.75 and 0.85 for TSS and 0.68 and 0.49 for anthocyanins at the bunch and vine level, respectively; this highlights the suitability of snapshot systems for robotic harvesting applications when rapid spatial mapping and automated detection tasks are prioritised. However, snapshot sensors face intrinsic limitations when deployed on moving platforms: the simultaneous acquisition of spatial and spectral information across the entire field of view increases sensitivity to motion blur and platform vibrations, potentially compromising spectral fidelity and spatial consistency during on-the-go operation. In contrast, the pushbroom scanning approach adopted in the present study enables continuous, high-throughput spectral acquisition along entire vine rows, proving particularly advantageous for developing robust calibration models under heterogeneous and dynamically changing field conditions.

A practical limitation of the present workflow is its reliance on manual basal leaf removal to ensure unobstructed cluster visibility prior to hyperspectral acquisition. Whilst this intervention enabled consistent spectral data collection, it may limit the scalability of routine on-the-go monitoring in commercial vineyards. Cluster occlusion by canopy foliage is a well-documented challenge for proximal sensing technologies, particularly in vertically shoot-positioned (VSP) training systems where seasonal canopy growth progressively reduces direct line-of-sight access to fruit pixels (Íñiguez *et al.,* 2024). A more operationally viable approach could involve coordinating hyperspectral monitoring campaigns with standard commercial defoliation practices, which are already performed in many wine regions. For instance, Fernández-Novales *et al.* (2019) successfully conducted on-the-go VNIR-SWIR measurements in 'Tempranillo' vineyards following routine late-July leaf removal, a common practice in Rioja DOCa aimed at improving cluster microclimate during ripening. However, whether prediction models calibrated under the full defoliation conditions employed in the present study would maintain comparable accuracy when applied to partially defoliated commercial canopies remains to be validated. Assessing model performance across varying degrees of canopy density and exploring multi-angle or dual-sided imaging approaches could mitigate occlusion effects.

The findings presented here have direct implications for adaptive harvest management under the increasingly variable climatic conditions affecting viticulture worldwide. Climate change is progressively narrowing the optimal harvest window and complicating traditional maturity assessment practices (van Leeuwen & Destrac-Irvine, 2017). The ability to simultaneously monitor sugar accumulation, organic acid dynamics, and phenolic development through on-the-go hyperspectral imaging enables more informed, data-driven harvest timing decisions that can preserve varietal typicity and wine style consistency across seasons of varying environmental conditions. For 'Tempranillo' – an early-ripening cultivar particularly vulnerable to climate-driven imbalances (Ramos & de Toda, 2021) – the operational deployment of such tools could support the identification of optimal harvest dates that balance moderate alcohol levels with adequate phenolic extraction and acid retention, thereby maintaining the region's signature wine profile despite increasing thermal stress.

In light of these implications, several research directions emerge that could further enhance the robustness, transferability, and operational utility of on-the-go hyperspectral monitoring systems. Multi-season, multi-site validation across diverse vintages and terroirs is essential for assessing model stability and evaluate recalibration requirements under varying environmental and agronomic conditions. In parallel, extending the methodology to individual secondary metabolites (for instance, phenolic and volatile compounds, amino acids, and polysaccharides) would enable a more comprehensive characterisation of grape biochemical composition within non-destructive monitoring frameworks. Advanced modelling strategies, including machine learning and deep learning architectures, should be evaluated to complement linear approaches where non-linear relationships dominate, whilst preserving model interpretability and operational robustness; additionally, the generation of spatial and temporal maps of grape composition evolution would allow dynamic visualisation of maturity gradients within and between vineyard blocks, supporting terroir-based management strategies and enabling selective harvesting according to ripeness heterogeneity.

Collectively, these findings confirm that dual-range on-the-go hyperspectral imaging can reliably quantify the technological maturity profile of 'Tempranillo' under field conditions, with prediction accuracy for sugar-acid balance parameters that matches or exceeds previous vineyard-based studies, whilst enabling meaningful assessment of nitrogen status and phenolic attributes. The developed workflow demonstrates that pushbroom acquisition systems, when combined with appropriate radiometric correction and chemometric calibration, can overcome the technical challenges of field spectroscopy, supporting the transition from laboratory proof-of-concept to operational field deployment in precision viticulture systems.

CONCLUSIONS

This study demonstrates that dual-range (VNIR-SWIR, 400–1700 nm) on-the-go hyperspectral imaging can accurately predict key grape composition parameters in *Vitis vinifera* L. cv. Tempranillo under real vineyard conditions, thus allowing a practical workflow for non-destructive maturity monitoring to be established at vine and block scales.

Technological maturity parameters achieved excellent quantitative prediction performance across all key attributes that govern sugar-acid balance, including total soluble solids, pH, and titratable acidity. The particularly robust prediction of malic acid is especially significant, given its strong temperature sensitivity during ripening; hyperspectral sensing thus has high potential for being a valuable tool for climate-adaptive harvest management under the increasing thermal stress and inter-annual variability affecting contemporary viticulture. Tartaric acid, whilst exhibiting greater stability throughout ripening, nonetheless achieved good quantitative prediction.

Beyond primary metabolites, this work represents the first successful field-based estimation of yeast-assimilable nitrogen, providing an innovative screening tool to guide fermentation management. Furthermore, the system demonstrated robust capabilities for tracking phenolic and chromatic parameters throughout grape ripening. Although predictive accuracy varied, highlighting the influence of different reference extraction protocols on anthocyanin estimation, colour indices, and total phenolic content were consistently well modelled.

Under the increasingly variable climatic conditions projected for viticultural regions, the potential for such spatially resolved monitoring becomes essential for preserving varietal identity, maintaining *terroir* expression, and safeguarding wine quality across uncertain growing seasons. In the context of premium Designations of Origin such as Rioja, where stylistic consistency and typicity are foundational to market positioning, the ability to objectively track the decoupling of technological and phenolic maturity – a phenomenon exacerbated by warming trends – provides critical decision support for harvest timing that balances sugar-acid dynamics with phenolic and aromatic development.

ACKNOWLEDGEMENTS

This work was carried out within the framework of the HyperGrape project (PID2023-150555OB-I00), and was funded by the Spanish Ministry of Science, Innovation and Universities (MCIU), the State Research Agency (AEI/10.13039/501100011033), and the European Regional Development Fund (ERDF/FEDER, EU).

The authors gratefully acknowledge the University of La Rioja and the Institute of Grapevine and Wine Sciences (ICVV) for the resources and facilities made available for this study. We also extend our sincere thanks to the vineyard manager for his collaboration regarding the use of the experimental site.

Aitana Tejada-González and Ignacio Barrio would like to express their gratitude for the financial support received through their respective predoctoral grants: PREP2023-001668, funded by MCIU/AEI/10.13039/501100011033/FSE+ (A.T.G.), and 887/2025, funded by Universidad de La Rioja and Gobierno de La Rioja (I.B.).

REFERENCES

Agati, G., Meyer, S., Matteini, P., & Cerović, Z. G. (2007). Assessment of anthocyanins in grape (Vitis vinifera L) berries using a noninvasive chlorophyll fluorescence method. *Journal of Agricultural and Food Chemistry*, *55*(4), 1053 – 1061. https://doi.org/10.1021/jf062956k

Aleixandre-Tudo, J. L., Nieuwoudt, H., Olivieri, A., Aleixandre, J. L., & du Toit, W. (2018). Phenolic profiling of grapes, fermenting samples and wines using UV-Visible spectroscopy with chemometrics. *Food Control*, *85*, 11–22. https://doi.org/10.1016/j.foodcont.2017.09.014

Allamy, L., Van Leeuwen, C., & Pons, A. (2023). Impact of harvest date on aroma compound composition of Merlot and Cabernet-Sauvignon must and wine in a context of climate change: a focus on cooked fruit molecular markers. *Oeno One*, *57*(3), 99 – 112. https://doi.org/10.20870/oeno-one.2023.57.3.7458

Alonso, J., Aranda, M., Córdoba, M. G., Ruiz-Moyano, S., Velázquez, R., Aranda, E., & Martín, A. (2026). VIS–SWIR hyperspectral imaging for campaign-year verification and moisture screening in smoked paprika (Capsicum annuum L.). *Journal of Food Composition and Analysis*, *153*, 109097. https://doi.org/10.1016/j.jfca.2026.109097

Amigo, J. M., Martí, I., & Gowen, A. A. (2013). Hyperspectral Imaging and Chemometrics. A Perfect Combination for the Analysis of Food Structure, Composition and Quality. In *Data Handling in Science and Technology* (Vol. 28, pp. 343 – 370). Elsevier. https://doi.org/10.1016/B978-0-444-59528-7.00009-0

Anderson, K., Nelgen, S., & Puga, G. (2024). Varietal Distinctiveness of World's Wine Regions: An Updated Empirical Picture. *IVES Technical Reviews, Vine and Wine*. https://doi.org/10.20870/IVES-TR.2024.8055

Baiano, A., Terracone, C., Peri, G., & Romaniello, R. (2012). Application of hyperspectral imaging for prediction of physico-chemical and sensory characteristics of table grapes. *Computers and Electronics in Agriculture*, *87*, 142 – 151. https://doi.org/10.1016/j.compag.2012.06.002

Baluja, J., Tardaguila, J., Ayestarán, B. M., & Diago, M. P. (2013). Spatial variability of grape composition in a Tempranillo (Vitis vinifera L.) vineyard over a 3-year survey. *Precision Agriculture*, *14*(1), 40 – 58. https://doi.org/10.1007/s11119-012-9282-5

Barnes, R. J., Dhanoa, M. S., & Lister, S. J. (1989). Standard normal variate transformation and de-trending of near-infrared diffuse reflectance spectra. *Applied Spectroscopy*, *43*(5), 772 – 777. https://doi.org/10.1366/0003702894202201

Bell, S.-J., & Henschke, P. (2005). Implications of nitrogen nutrition for grapes, fermentation and wine. *Australian Journal of Grape and Wine Research*, *11*(3), 242–295. https://doi.org/10.1111/j.1755-0238.2005.tb00028.x

Benelli, A., Cevoli, C., Fabbri, A., Engelsen, S. B., & Sorensen, K. M. (2024). Precision viticulture: Automatic selection of the regions of interest from moving wagon hyperspectral images of grapes for efficient SSC prediction. *Smart Agricultural Technology*, *7,* 100434. https://doi.org/10.1016/j.atech.2024.100434

Benelli, A., Cevoli, C., Ragni, L., & Fabbri, A. (2021). In-field and non-destructive monitoring of grapes maturity by hyperspectral imaging. *Biosystems Engineering*, *207*, 59 – 67. https://doi.org/10.1016/j.biosystemseng.2021.04.006

Bertoglio, R., Piliego, M., Guadagna, P., Gatti, M., Poni, S., & Matteucci, M. (2024). On-the-go table grape ripeness estimation via proximal snapshot hyperspectral imaging. *Computers and Electronics in Agriculture*, *226*, 109354. https://doi.org/10.1016/j.compag.2024.109354

Bramley, R. G. V., Ouzman, J., & Trought, M. C. T. (2020). Making sense of a sense of place: precision viticulture approaches to the analysis of terroir at different scales. *OENO One*, *54*(4), 903 – 917. https://doi.org/10.20870/oeno-one.2020.54.4.3858

Bramley, R. G. V., Pearse, B., & Chamberlain, P. (2003). Being profitable precisely-a case study of precision viticulture from Margaret River. *Australian and New Zealand Grapegrower and Winemaker*, *473a*, 84 – 87.

Brown, C. D., Vega-Montoto, L. J., & Wentzell, P. D. (2000). Derivative preprocessing and optimal corrections for baseline drift in multivariate calibration. *Applied Spectroscopy*, *54*(7), 1055 – 1068. https://doi.org/10.1366/0003702001950571

Canals, R., Llaudy, M. C., Valls Fonayet, J., Canals, J.-M. M., & Zamora, F. (2005). Influence of ethanol concentration on the extraction of color and phenolic compounds from the skin and seeds of tempranillo grapes at different stages of ripening. *Journal of Agricultural and Food Chemistry*, *53*(10), 4019 – 4025. https://doi.org/10.1021/jf047872v

Cervera, M. T., Cabezas, J. A., Rodríguez-Torres, I., Chávez, J., Cabello, F., & Martinez-Zapater, J. M. (2002). Varietal diversity within grapevine accessions of cv. Tempranillo. *Vitis - Journal of Grapevine Research*, *41*(1), 33 – 36. https://doi.org/10.5073/vitis.2002.41.33-36

Çetin, N., Karaman, K., Kavuncuoğlu, E., Yıldırım, B., & Jahanbakhshi, A. (2022). Using hyperspectral imaging technology and machine learning algorithms for assessing internal quality parameters of apple fruits. *Chemometrics and Intelligent Laboratory Systems*, *230*, 104650. https://doi.org/10.1016/j.chemolab.2022.104650

Chen, S., Zhang, F., Ning, J., Liu, X., Zhang, Z., & Yang, S. (2015). Predicting the anthocyanin content of wine grapes by NIR hyperspectral imaging. *Food Chemistry*, *172*, 788 – 793. https://doi.org/10.1016/j.foodchem.2014.09.119

Cornelissen, C., Coninck, S. De, Willekens, A., Leroux, S., & Simoens, P. (2025). In-Field Mapping of Grape Yield and Quality with Illumination-Invariant Deep Learning. *IEEE Internet of Things Journal*. https://doi.org/10.1109/JIOT.2025.3617805

Cosme, F., Filipe-Ribeiro, L., & Nunes, F. M. (2024). Introductory chapter: Impact of Climate Change on Grapes and Grape Products. In *Global Warming and the Wine Industry - Challenges, Innovations and Future Prospects*. IntechOpen. https://doi.org/10.5772/intechopen.1005092

Cozzolino, D., Dambergs, R. G., Janik, L., Cynkar, W. U., & Gishen, M. (2006). Analysis of Grapes and Wine by near Infrared Spectroscopy. *Journal of Near Infrared Spectroscopy*, *14*(5), 279–289. https://doi.org/10.1255/jnirs.679

Dale, L. M., Thévis, A., Boudry, C., Rotar, I., Dardenne, P., Baeten, V., & Fernández Pierna, J. A. (2013). Hyperspectral imaging applications in agriculture and agro-food product quality and safety control: A review. *Applied Spectroscopy Reviews*, *48*(2), 142 – 159. https://doi.org/10.1080/05704928.2012.705800

Droulia, F. E., & Charalampopoulos, I. (2021). Future climate change impacts on european viticulture: A review on recent scientific advances. *Atmosphere*, *12*(4), 495. https://doi.org/10.3390/atmos12040495

ElMasry, G. M., & Sun, D. W. (2010). Principles of Hyperspectral Imaging Technology. In *Hyperspectral imaging for food quality analysis and control* (pp. 3 – 43). https://doi.org/10.1016/B978-0-12-374753-2.10001-2

Fernandes, A. M., Oliveira, P. C. R. C., Moura, J. P., Oliveira, A. A., Falco, V., Correia, M. J., & Melo-Pinto, P. (2011). Determination of anthocyanin concentration in whole grape skins using hyperspectral imaging and adaptive boosting neural networks. *Journal of Food Engineering*, *105*(2), 216 – 226. https://doi.org/10.1016/j.jfoodeng.2011.02.018

Fernández-Novales, J., Barrio, I., & Diago, M. P. (2021). Non-invasive monitoring of berry ripening using on-the-go hyperspectral imaging in the vineyard. *Agronomy*, *11*(12), 2534. https://doi.org/10.3390/agronomy11122534

Fernández-Novales, J., Tardáguila, J., Gutiérrez, S., & Diago, M. P. (2019). On-The-Go VIS + SW − NIR Spectroscopy as a Reliable Monitoring Tool for Grape Composition within the Vineyard. *Molecules*, *24*(15), 2795. https://doi.org/10.3390/molecules24152795

Gabrielli, M., Ounaissi, D., Lancon-Verdier, V., Julien, S., Le Meurlay, D., & Maury, C. (2023). Hyperspectral imaging to assess wine grape quality. *JSFA Reports*, *3*(10), 452 – 462. https://doi.org/10.1002/jsf2.150

Gao, S., & Xie, W. (2024). SSC and pH prediction and maturity classification of grapes based on hyperspectral imaging. *Smart Agricultural Technology*, *8,* 100457. https://doi.org/10.1016/j.atech.2024.100457

Gao, S., & Xu, J. (2022). Hyperspectral image information fusion-based detection of soluble solids content in red globe grapes. *Computers and Electronics in Agriculture*, *196,* 106822. https://doi.org/10.1016/j.compag.2022.106822

Gao, S., & Xu, J. (2024). Non-destructive detection of total acid of red globe grapes based on map fusion technique. *Smart Agricultural Technology*, *7,* 100406. https://doi.org/10.1016/j.atech.2024.100406

Garrido, J., & Borges, F. (2013). Wine and grape polyphenols — A chemical perspective. *Food Research International*, *54*(2), 1844–1858. https://doi.org/10.1016/j.foodres.2013.08.002

Glories, Y. (1984). La couleur des vins rouges. lre partie : les équilibres des anthocyanes et des tanins. *Oeno One*, *18*(3), 195–217. https://doi.org/10.20870/oeno-one.1984.18.3.1751

Goetz, A. F. H., Vane, G., Solomon, J. E., & Rock, B. N. (1985). Imaging spectrometry for earth remote sensing. *Science*, *228*(4704), 1147 – 1153. https://doi.org/10.1126/science.228.4704.1147

Gomes, V. M., Fernandes, A. M., Mendes-Faia, A., & Melo-Pinto, P. (2017). Comparison of different approaches for the prediction of sugar content in new vintages of whole Port wine grape berries using hyperspectral imaging. *Computers and Electronics in Agriculture*, *140*, 244 – 254. https://doi.org/10.1016/j.compag.2017.06.009

González-Pavez, M. I., Ortega-Farías, S. O., Poblete-Echeverria, C. A., Gamboa, M. J., & Vargas, S. (2025). Application of spectral index-based contour mapping for non-destructive ripeness monitoring in water stressed Vitis vinifera L. (Cabernet-Sauvignon). *Oeno One*, *59*(2). https://doi.org/10.20870/oeno-one.2025.59.2.9308

Gowen, A. A., O'Donnell, C. P., Cullen, P. J., Downey, G. A., & Celayeta, J. M. F. (2007). Hyperspectral imaging - an emerging process analytical tool for food quality and safety control. *Trends in Food Science and Technology*, *18*(12), 590 – 598. https://doi.org/10.1016/j.tifs.2007.06.001

Gutiérrez, S., Tardaguila, J., Fernández-Novales, J., & Diago, M. P. (2019). On-the-go hyperspectral imaging for the in-field estimation of grape berry soluble solids and anthocyanin concentration. *Australian Journal of Grape and Wine Research*, *25*(1), 127 – 133. https://doi.org/10.1111/ajgw.12376

Gutiérrez, S., Wendel, A., & Underwood, J. (2019). Ground based hyperspectral imaging for extensive mango yield estimation. *Computers and Electronics in Agriculture*, *157*, 126–135. https://doi.org/10.1016/j.compag.2018.12.041

Hall, A., Lamb, D. W., Holzapfel, B. P., & Louis, J. P. (2002). Optical remote sensing applications in viticulture - A review. *Australian Journal of Grape and Wine Research*, *8*(1), 36 – 47. https://doi.org/10.1111/j.1755-0238.2002.tb00209.x

He, M., Li, C., Cai, Z., Qi, H., Zhou, L., & Zhang, C. (2024). Leafy vegetable freshness identification using hyperspectral imaging with deep learning approaches. *Infrared Physics & Technology*, *138*, 105216. https://doi.org/10.1016/j.infrared.2024.105216

Helland, I. S. (2001). Some theoretical aspects of partial least squares regression. *Chemometrics and Intelligent Laboratory Systems*, *58*(2), 97 – 107. https://doi.org/10.1016/S0169-7439(01)00154-X

Ibáñez, J., Muñoz-Organero, G., Zinelabidine, L. H., Teresa de Andrés, M., Cabello, F., & Martinez-Zapater, J. M. (2012). Genetic origin of the grapevine cultivar tempranillo. *American Journal of Enology and Viticulture*, *63*(4), 549 – 553. https://doi.org/10.5344/ajev.2012.12012

Iland, P., Bruer, N., Edwards, G., Weeks, S., & Wilkes, E. (2004). *Chemical Analysis of Grapes and Wine: Techniques and Concepts*. Patrick Iland Wine Promotions Pty Ltd.

Iland, P., Dry, P., Proffitt, T., Tyerman, S., Collins, C., Pagay, V., & Steel, C. (2024). *The grapevine: From the science to the practice of growing vines for wine*. Patrick Iland Wine Promotions Pty Ltd.

Íñiguez, R., Gutiérrez, S., Poblete-Echeverría, C., Hernández, I., Barrio, I., & Tardáguila, J. (2024). Deep learning modelling for non-invasive grape bunch detection under diverse occlusion conditions. *Computers and Electronics in Agriculture*, *226*, 109421. https://doi.org/10.1016/j.compag.2024.109421

Jin, C., Zhou, L., Zhao, Y., Qi, H., Wu, X., & Zhang, C. (2025). Classification of rice varieties using hyperspectral imaging with multi-dimensional fusion convolutional neural networks. *Journal of Food Composition and Analysis*, *148*, 108389. https://doi.org/10.1016/j.jfca.2025.108389

Jones, G. V, Edwards, E. J., Bonada, M., Sadras, V. O., Krstic, M. P., & Herderich, M. J. (2022). Climate change and its consequences for viticulture. In *Managing Wine Quality* (pp. 727–778). Elsevier. https://doi.org/10.1016/B978-0-08-102067-8.00015-4

Khiari, R., Ounaissi, D., Lancon-Verdier, V., Zemni, H., Mihoubi, D., & Maury, C. (2025). Ability of hyperspectral imaging to assess physicochemical and phytochemical quality parameters of raisins. *Journal of Food Measurement and Characterization*, *19*(2), 1234 – 1247. https://doi.org/10.1007/s11694-024-03036-1

Kim, M.-J., Yu, W.-H., Song, D.-J., Chun, S.-W., Kim, M. S., Lee, A., Kim, G., Shin, B.-S., & Mo, C. (2024). Prediction of Soluble-Solid Content in Citrus Fruit Using Visible–Near-Infrared Hyperspectral Imaging Based on Effective-Wavelength Selection Algorithm. *Sensors*, *24*(5), 1512. https://doi.org/10.3390/s24051512

Lorenz, D. H., Eichhorn, K. W., Bleiholder, H., Klose, R., Meier, U., & Weber, E. (1995). Growth Stages of the Grapevine: Phenological growth stages of the grapevine (Vitis vinifera L. ssp. vinifera)—Codes and descriptions according to the extended BBCH scale. *Australian Journal of Grape and Wine Research*, *1*(2), 100–103. https://doi.org/10.1111/j.1755-0238.1995.tb00085.x

Lorrain, B., Ky, I., Péchamat, L., & Teissedre, P. L. (2013). Evolution of analysis of polyhenols from grapes, wines, and extracts. *Molecules*, *18*(1), 1076 – 1100. https://doi.org/10.3390/molecules18011076

Marín-San Román, S., Diago, M. P., Fernández-Novales, J., Cebrián-Tarancón, C., Salinas, M. R., & Garde-Cerdán, T. (2024). Use of the hyperspectral imaging to estimate the volatile composition of Tempranillo grape berries during ripening. *Scientia Horticulturae*, *337,* 113537. https://doi.org/10.1016/j.scienta.2024.113537

Minnaar, P. P., van der Rijst, M., & Hunter, J. J. (2022). Grapevine row orientation, vintage and grape ripeness effect on anthocyanins, flavan-3-ols, flavonols and phenolic acids: I. Vitis vinifera L. cv. Syrah grapes. *Oeno One*, *56*(1), 275 – 293. https://doi.org/10.20870/oeno-one.2022.56.1.4857

Mishra, G., Panda, B. K., Ramirez, W. A., Jung, H., Singh, C. B., Lee, S.-H., & Lee, I. (2022). Application of SWIR hyperspectral imaging coupled with chemometrics for rapid and non-destructive prediction of Aflatoxin B1 in single kernel almonds. *LWT*, *155*, 112954. https://doi.org/10.1016/j.lwt.2021.112954

Nazir, A., AlDhaheri, M., Mudgil, P., Marpu, P., & Kamal-Eldin, A. (2022). Hyperspectral imaging based kinetic approach to assess quality deterioration in fresh mushrooms (Agaricus bisporus) during postharvest storage. *Food Control*, *131*, 108298. https://doi.org/10.1016/j.foodcont.2021.108298

Nogales-Bueno, J., Hernández Hierro, J. M., Rodríguez-Pulido, F. J., & Heredia, F. J. (2014). Determination of technological maturity of grapes and total phenolic compounds of grape skins in red and white cultivars during ripening by near infrared hyperspectral image: A preliminary approach. *Food Chemistry*, *152*, 586 – 591. https://doi.org/10.1016/j.foodchem.2013.12.030

OIV. (2024). *Compendium of International Methods of Wine and Must Analysis*. International Organisation of Vine and Wine.

Pasquini, C. (2018). Near infrared spectroscopy: A mature analytical technique with new perspectives – A review. *Analytica Chimica Acta*, *1026*, 8–36. https://doi.org/10.1016/j.aca.2018.04.004

Piazzolla, F., Amodio, M. L., & Colelli, G. (2017). Spectra evolution over on-vine holding of italia table grapes: Prediction of maturity and discrimination for harvest times using a Vis-NIR hyperspectral device. *Journal of Agricultural Engineering*, *48*(2), 109 – 116. https://doi.org/10.4081/jae.2017.639

Plantevin, M., Merpault, Y., Lecourt, J., Destrac-Irvine, A., Dijsktra, L., & Van Leeuwen, C. (2024). Characterization of varietal effects on the acidity and pH of grape berries for selection of varieties better adapted to climate change. *Frontiers in Plant Science*, *15,* 1439114. https://doi.org/10.3389/fpls.2024.1439114

Poni, S., Casalini, L., Bernizzoni, F., Civardi, S., & Intrieri, C. (2006). Effects of early defoliation on shoot photosynthesis, yield components, and grape composition. *American Journal of Enology and Viticulture*, *57*(4), 397 – 407. https://doi.org/10.5344/ajev.2006.57.4.397

Ramos, M. C., & Martinez de Toda, F. M. De. (2020). Variability in the potential effects of climate change on phenology and on grape composition of Tempranillo in three zones of the Rioja DOCa (Spain). *European Journal of Agronomy*, *115,* 126014. https://doi.org/10.1016/j.eja.2020.126014

Ramos, M. C., & Martinez de Toda, F. M. De. (2021). Interannual and spatial variability of grape composition in the Rioja DOCa show better resilience of cv. Graciano than cv. Tempranillo under a warming scenario. *Oeno One*, *55*(3), 85 – 100. https://doi.org/10.20870/oeno-one.2021.55.3.4695

Rienth, M., Vigneron, N., Darriet, P., Sweetman, C., Burbidge, C., Bonghi, C., Walker, R. P., Famiani, F., & Castellarin, S. D. (2021). Grape Berry Secondary Metabolites and Their Modulation by Abiotic Factors in a Climate Change Scenario–A Review. *Frontiers in Plant Science*, *12,* 643258. https://doi.org/10.3389/fpls.2021.643258

Rinnan, Å., Berg, F. Van Den, & Engelsen, S. B. (2009). Review of the most common pre-processing techniques for near-infrared spectra. *TrAC - Trends in Analytical Chemistry*, *28*(10), 1201 – 1222. https://doi.org/10.1016/j.trac.2009.07.007

Sadras, V. O., & Moran, M. A. (2012). Elevated temperature decouples anthocyanins and sugars in berries of Shiraz and Cabernet Franc. *Australian Journal of Grape and Wine Research*, *18*(2), 115 – 122. https://doi.org/10.1111/j.1755-0238.2012.00180.x

Sams, B., Bramley, R. G. V, Sanchez, L., Dokoozlian, N. K., Ford, C. M., & Pagay, V. (2022). Characterising spatio-temporal variation in fruit composition for improved winegrowing management in California Cabernet Sauvignon. *Australian Journal of Grape and Wine Research*, *28*(3), 407–423. https://doi.org/10.1111/ajgw.12542

Savitzky, A., & Golay, M. J. E. (1964). Smoothing and Differentiation of Data by Simplified Least Squares Procedures. *Analytical Chemistry*, *36*(8), 1627 – 1639. https://doi.org/10.1021/ac60214a047

Shenk, J. S., & Westerhaus, M. O. (1995). *Routine operation, calibration, development and network system management manual*. NIRSystems Inc.

Siedliska, A., Krzyszczak, J., Baranowski, P., Banach, A., Siłuch, M., Bartmiński, P., Wolińska, A., & Tkaczyk, P. (2026). Can Hyperspectral Imaging be Used for Rapid Monitoring of Potassium Content in Sugar Beet and Celery? *Journal of Soil Science and Plant Nutrition*, *26*(1), 3861–3883. https://doi.org/10.1007/s42729-026-03103-0

Tardaguila, J., Stoll, M., Gutiérrez, S., Proffitt, T., & Diago, M. P. (2021). Smart applications and digital technologies in viticulture: A review. *Smart Agricultural Technology*, *1,* 100005. https://doi.org/10.1016/j.atech.2021.100005

Tsakiridis, N. L., Samarinas, N., Kokkas, S., Kalopesa, E., Tziolas, N. V., & Zalidis, G. C. (2023). In situ grape ripeness estimation via hyperspectral imaging and deep autoencoders. *Computers and Electronics in Agriculture*, *212*, 108098. https://doi.org/10.1016/j.compag.2023.108098

van Leeuwen, C., & Destrac-Irvine, A. (2017). Modified grape composition under climate change conditions requires adaptations in the vineyard. *Oeno One*, *51*(2), 147 – 154. https://doi.org/10.20870/oeno-one.2016.0.0.1647

van Leeuwen, C., Destrac-Irvine, A., Dubernet, M., Duchêne, É., Gowdy, M., Marguerit, E., Pieri, P., Parker, A. K., de Rességuier, L., & Ollat, N. (2019). An update on the impact of climate change in viticulture and potential adaptations. *Agronomy*, *9*(9), 514. https://doi.org/10.3390/agronomy9090514

van Leeuwen, C., Sgubin, G., Bois, B., Ollat, N., Swingedouw, D., Zito, S., & Gambetta, G. A. (2024). Climate change impacts and adaptations of wine production. *Nature Reviews Earth & Environment*, *5*(4), 258–275. https://doi.org/10.1038/s43017-024-00521-5

Verdugo-Vásquez, N., Acevedo-Opazo, C., Valdés-Gómez, H., la Fuente, C. P.-D., Ingram, B., de Cortázar-Atauri, I. G., & Tisseyre, B. (2022). Identification of main factors affecting the within-field spatial variability of grapevine phenology and total soluble solids accumulation: towards the vineyard zoning using auxiliary information. *Precision Agriculture*, *23*(1), 253–277. https://doi.org/10.1007/s11119-021-09836-5

Williams, P., & Norris, K. H. (2001). *Near-infrared technology: in the agricultural and food industries*. American Association of Cereal Chemists.

Wold, S., Sjöström, M., & Eriksson, L. (2001). PLS-regression: A basic tool of chemometrics. *Chemometrics and Intelligent Laboratory Systems*, *58*(2), 109 – 130. https://doi.org/10.1016/S0169-7439(01)00155-1

Xu, M., Sun, J., Cheng, J., Yao, K., Wu, X., & Zhou, X. (2023). Non-destructive prediction of total soluble solids and titratable acidity in Kyoho grape using hyperspectral imaging and deep learning algorithm. *International Journal of Food Science and Technology*, *58*(1), 9 – 21. https://doi.org/10.1111/ijfs.16173

Ye, W., Xu, W., Yan, T., Yan, J., Gao, P., & Zhang, C. (2023). Application of Near-Infrared Spectroscopy and Hyperspectral Imaging Combined with Machine Learning Algorithms for Quality Inspection of Grape: A Review. *Foods*, *12*(1), 132. https://doi.org/10.3390/foods12010132

Zhang, D., Xu, L., Liang, D., Xu, C., Jin, X., & Weng, S. (2018). Fast Prediction of Sugar Content in Dangshan Pear (Pyrus spp.) Using Hyperspectral Imagery Data. *Food Analytical Methods*, *11*(8), 2336–2345. https://doi.org/10.1007/s12161-018-1212-3

Zhang, Y., Li, X., Wang, M., Xu, T., Huang, K., Sun, Y., Yuan, Q., Lei, X., Qi, Y., & Lv, X. (2024). Early detection and lesion visualization of pear leaf anthracnose based on multi-source feature fusion of hyperspectral imaging. *Frontiers in Plant Science*, *15,* 1461855. https://doi.org/10.3389/fpls.2024.1461855

Zhao, Z., Cao, W., Fang, L., Chen, M., Liu, X., Qiu, J., Ma, L., Dong, W., & Zhao, X. (2026). Determination of firmness, soluble tannin content, and storage stage of post-harvest astringent persimmons using VNIR-SWIR hyperspectral imaging and deep learning. *Journal of Food Composition and Analysis*, *150*, 108848. https://doi.org/10.1016/j.jfca.2025.108848